[CO-REGISTRATION BETWEEN IMAGERY AND POINT CLOUD ACQUIRED BY MLS PLATFORM]
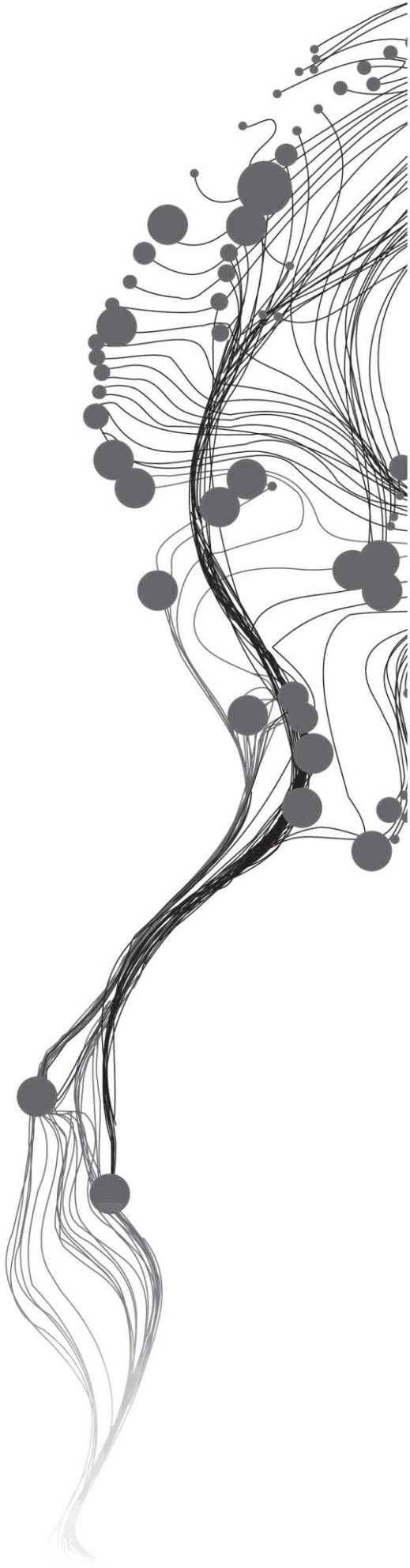
[FANGNING HE]
[FEBRUARY, 2012]

SUPERVISORS:

[Professor, Dr. Ir. M.G. Vosselman]
[Doctor, M. Gerke]

[CO-REGISTRATION BETWEEN IMAGERY AND POINT CLOUD ACQUIRED BY MLS PLATFORM]

[FANGNING HE]
Enschede, The Netherlands, [February, 2012]

Thesis submitted to the Faculty of Geo-Information Science and Earth Observation of the University of Twente in partial fulfilment of the requirements for the degree of Master of Science in Geo-information Science and Earth Observation.
Specialization: [Geoinformatics]

SUPERVISORS:
[Prof.Dr.Ir. M.G. Vosselman]
[Dr. M. Gerke]

THESIS ASSESSMENT BOARD:
[Prof. M.J. Kraak (Chair)]
[Dr. R.C. Lindenbergh (External Examiner, Delft University of Technology)]

ABSTRACT

Over the past few years, the mobile laser scanning (MLS) system which can simultaneously obtain the imagery and the point cloud data has been widely used in various areas. In most cases, to enable further applications, both the imagery and point cloud data acquired by the same MLS platform has to be registered into one common coordinate system. To solve this problem, a direct geo-referencing procedure is carried out. In this procedure, the orientations of both the camera and the laser scanner can be reconstructed with the information of GPS/IMU data. However, in some cases, due to the inaccurate system mounting parameters, the orientations of each sensor can be poorly reconstructed, and the co-registration between the imagery and the point cloud data may be also affected.

In this thesis, a two-step calibration procedure is introduced. The aim of this procedure is to find the potential error sources that may influence the co-registration quality between imagery and point cloud data. In the first step of this proposed procedure, an indirect co-registration method is developed to estimate the orientation of the camera with respect to the geo-referenced point cloud data. In this co-registration method, first, the images are relatively oriented by using a free network adjustment, then a 3D similarity transformation which uses point features, line features and plane features are applied to complete the transformation from the image space to the object space. Based on this method, the exterior orientation parameters of the camera can be reconstructed in the mapping coordinate system. In the second step of this proposed procedure, both the reconstructed exterior orientation parameters and the original exterior orientation parameters derived from direct geo-referencing are utilized together for the bias estimation on the boresight angles and lever-arm offsets. By using the estimated bias, the orientation between the camera and the geo-referenced point cloud data can be corrected, and the co-registration quality between the imagery and the point cloud data can be improved.

The proposed two-step procedure is tested on the selected experimental data in this research, and a detailed analysis for the testing result is also presented in this thesis. Based on the analysis, several recommendations on improving the accuracy of final result have been given. In the meantime, the possibility of applying this proposed procedure to actual applications has also been demonstrated in this research.

Keywords: Mobile Laser Scanning system, Co-registration, 3D similarity transformation, Bias estimation, Boresight alignment, Lever-arm offsets

ACKNOWLEDGEMENTS

TABLE OF CONTENTS

LIST OF FIGURES

LIST OF TABLES

1. INTRODUCTION

1.1. Motivation and problem statement

"Laser scanning is a relatively young 3D measurement technique offering much potential in the acquisition of precise and reliable 3D geo-data and object geometries" (Vosselman & Maas, 2010). Compared with traditional optical surveying techniques, laser scanning can be time-efficient and cost-efficient as well as with a higher accuracy. As an effective alternative to conventional surveying methods, accurate 3D point clouds data acquired by laser scanning system have been widely used for different purposes including transportation planning, forest monitoring, digital mapping and so forth.

Sometimes, to enable a much faster and more efficient 3-D data acquisition process, the laser scanner will be deployed on a mobile platform, such as a car, a boat or an all-terrain vehicle, to build up a mobile laser scanning system (Kaasalainen et al., 2011). And this mobile laser scanning technique has become an important tool in a great number of fields, such as traffic monitoring, railway surveying and urban modelling. In the meantime, with the development and improvement of platforms, current mobile laser scanning system, which integrated digital cameras and laser scanners, could obtain geo-referenced point clouds data as well as imageries simultaneously.
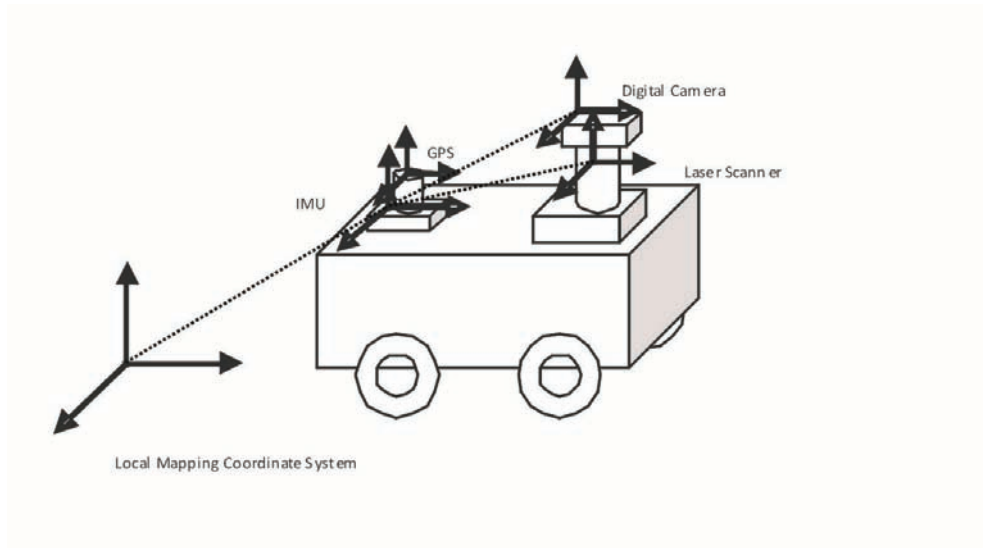
Figure 1.1 Relationship between different sensors and devices

This kind of multi-sensor Mobile Mapping System usually comprises a position and orientation system (POS), which includes a global positioning system (GPS) receiver and an inertial measurement unit (IMU). In this system, the GPS provides position and velocity of the platform, and the IMU provides attitude or orientation of the sensor with respect to the ground (Haala et al., 2008; Habib et al., 2008). With these data, software could automatically interpolate the attitude and location of platform at each scanning or exposure moment. Meanwhile, the trajectory of mobile platform could be reconstructed as well. On the other hand, since the laser scanner, digital cameras and POS are rigidly mounted on the same platform, the relative geometric relationship could be determined from system calibration. As a result, all the sensors

and devices could be integrated into one common local-mapping coordinate system. Figure 1 illustrates the relationship between different sensors and devices. And the whole procedure is called direct geo-referencing (Manandhar & Shibasaki, 2000; Mostafa & Schwarz, 2001).

After applying the procedure of direct geo-referencing, the local mapping coordinates of each laser scanning point could be computed, and the exterior orientation parameters of each image could also be determined. Therefore, these two different data sets could be co-registered together via conventional collinearity equations. However, there are several factors that may influence the quality of co-registration, such as the quality of individual sensor calibration and the quality of system mounting parameters. Current research has demonstrated that the final co-registration quality between laser scanning data and imageries is mainly limited by the quality of system calibration (Habib et al., 2010; Rau et al., 2011). Any error from the system mounting parameters like lever-arm offsets and boresight angles would directly propagate to the final co-registration result. For instance, even if the point cloud data acquired by the laser scanner is very accurately geo-referenced, a small lever-arm shift between camera and GPS/IMU frame, which results in a significant position error of camera projective center, would lead to a bad co-registration quality between point clouds data and imageries.

In fact, due to the different calibration qualities of different platforms, the final co-registration quality may vary from platform to platform. Especially, for an inaccurately calibrated MLS platform, the relative geometric relationship between digital camera and laser scanner could be very poorly estimated, and the final co-registration quality could also be influenced by inaccurate platform orientation between different sensors, like a boresight misalignment of digital camera. Therefore, how to model and eliminate theses potential error sources in an inaccurately calibrated MLS platform seems to be essential and important in current research.

1.2.   Research identification

1.2.1.   Research objectives

The primary objective of this research is to develop a procedure to model and correct potential error sources which may influence the co-registration quality in an inaccurately calibrated MLS platform. In this procedure, first, the exterior orientation parameters of imagery with respect to geo-referenced point cloud data are accurately determined, and then the accurately estimated exterior orientation parameters are compared with the original exterior orientation parameters which are derived in the direct geo-referencing procedure.

After applying the whole procedure, the accuracy of the relative orientation between imagery and geo-referenced point cloud data as well as the co-registration quality is expected to increase.

To achieve this objective, the whole research could be divided into several sub-objectives:

- Develop a procedure for the co-registration between imagery and point clouds data acquired by MLS platform.
- Establish a mathematical model for the estimation of bias which caused by inaccurate platform orientation
- Investigate the use of correspondent line features and plane features in the proposed procedure
- Evaluate the performance of the proposed procedure on real data

1.2.2. Research questions

For solving this research problem, several research questions need to be answered:

- How to check the error caused by radial distortion?
- How to recover the exterior orientation parameters of imageries based on point features?
- How to recover the exterior orientation parameters of imageries based on line features?
- How to recover the exterior orientation parameters of imageries based on plane features?
- Are there sufficient correspondent plane features allowing manually or automatically extraction from both point clouds data and imageries?
- What is the result of applying plane features in this proposed procedure?
- How to model the systematic errors caused by inaccurate platform orientation?
- How to evaluate the estimated bias derived in the proposed procedure?

1.3. Innovation aimed at

The innovations in this research are:
- No test field or surveyed targets are needed in this research.
- Besides point features, line features and plane features are used in this research for the co-registration between imagery and point cloud data.

1.4. Structure of thesis

To achieve the overall objective and answer all the above mentioned questions, the thesis is divided into 5 chapters.

Chapter 1: Introduction
This chapter includes motivation, problem statement, research objectives, research questions and the innovation aimed at in this research.
Chapter 2: Literature Review
This chapter includes the theoretical background for this research as well as a review of the related work in the literature. First the co-registration between imagery and point cloud data is introduced, and then the related techniques for platform calibration and system mounting parameters estimation are reviewed.
Chapter 3: Proposed Method
This chapter introduces the proposed two-step procedure in this research.
Chapter 4: Result and Analysis
This chapter describes the selected experiment data. The achieved results and analysis are also presented in this chapter.
Chapter 5: Conclusion and Recommendations
Conclusion of the research, answers to the research question and recommendations for further research are presented in this chapter.

2. LITERATURE REVIEW

2.1. Introduction

In this chapter, theoretical background needed for this research is presented. The chapter starts with the description of co-registration between imageries and point cloud data acquired by MLS platforms. An overview of current co-registration methods will be presented in section 2.2. Then, an overview of platform calibration is presented in section 2.3. Finally, a summary of previous research is presented in section 2.4

2.2. Co-registration between imagery and point cloud

To properly register imagery and point cloud data into one common coordinate system, the geometric relationship between different sensors needs to be recovered. A three dimensional Helmert transformation is generally used to establish this geometric relationship.

$$\begin{bmatrix} X \\ Y \\ Z \end{bmatrix} = s \cdot R \cdot \begin{bmatrix} x \\ y \\ -c \end{bmatrix} + \begin{bmatrix} X_0 \\ Y_0 \\ Z_0 \end{bmatrix} \qquad \text{Equation 2-1}$$

Where:

(x, y) is the coordinates in camera coordinate system;

(X, Y, Z) is the coordinates of geo-referenced laser point;

(X_0, Y_0, Z_0) is the coordinates of projection center of digital camera;

c is the focal length of digital camera;

s is the scale factor;

R is the rotation matrix from camera coordinate system to object coordinate system and could be expressed as three separate rotations along X, Y, Z axes.

$$R = \begin{bmatrix} \cos \kappa & -\sin \kappa & 0 \\ \sin \kappa & \cos \kappa & 0 \\ 0 & 0 & 1 \end{bmatrix} \cdot \begin{bmatrix} \cos \varphi & 0 & \sin \varphi \\ 0 & 1 & 0 \\ -\sin \varphi & 0 & \cos \varphi \end{bmatrix} \cdot \begin{bmatrix} 1 & 0 & 0 \\ 0 & \cos \omega & -\sin \omega \\ 0 & \sin \omega & \cos \omega \end{bmatrix} \qquad \text{Equation 2-2}$$

Where:

ω, φ, κ are three rotation angles with respect to X, Y, Z axis relating camera coordinate system to object coordinate system.

In the case of co-registration between imagery and point cloud data, the collinearity equation which describes the transformation from geo-referenced laser point (X, Y, Z) to image coordinates(x, y) could be directly derived from 3-D Helmert transformation model. The collinearity equation is given as follows:

$$\begin{cases} x = -c\dfrac{r_{11}(X - X_0) + r_{21}(Y - Y_0) + r_{31}(Z - Z_0)}{r_{13}(X - X_0) + r_{23}(Y - Y_0) + r_{33}(Z - Z_0)} \\ y = -c\dfrac{r_{12}(X - X_0) + r_{22}(Y - Y_0) + r_{32}(Z - Z_0)}{r_{13}(X - X_0) + r_{23}(Y - Y_0) + r_{33}(Z - Z_0)} \end{cases}$$

Equation 2-3

Where:

r_{ij} is the coefficient (i, j) in rotation matrix R.

In general, to properly orient an image in a mobile laser scanner platform, the exterior orientation parameters as well as interior orientation parameters of camera needs to be given. In the direct geo-referencing procedure, three translation parameters (X_0, Y_0, Z_0) which record the position of camera projection center could be directly interpolated from GPS/IMU data. However, the three rotation parameters derived from the navigation system are not in terms of Omega, Phi and Kappa which are used in normal photogrammetric system (Bäumker & Heimes, 2001). These three rotation parameters are given as roll, pitch and heading in the navigation coordinate system. Therefore, an additional transformation from the navigation coordinate system to the object coordinate system is needed. If the overall transformation is applied from image space to object space, the rotation sequences should be as follows: First rotate from the camera coordinate system to the platform body coordinate system; then rotate from the platform body coordinate system to the navigation coordinate system; finally rotate from the navigation coordinate system to the local mapping coordinate system.

As long as all these parameters in collinearity equation are reconstructed, the geo-referenced laser point could be back-projected onto correspondent image, and the coordinates of correspondent point on the image could be calculated as well.

Besides direct geo-referencing, several other methods have been also developed to properly orient images with geo-referenced point cloud data in a mobile multi-sensor platform. Al-Manasir and Fraser (2006) developed an automatic process to solve the spatial position and orientation of the camera within the laser scanner coordinate system. In this method, several identified coded targets needs to be placed on the object to apply a 3D similarity transformation. Rönnholm et al. (2009) presented two method for solving relative orientation between point cloud data and images. In the first method, a 3D model was derived from photogrammetric measurements, and then distances between point cloud data and the 3D model were minimized by using an ICP method. The second method utilized an interactive orientation method. In this method, digital images captured by different sensors were integrated into one multi-scale image block to improve the accuracy of orientation. González-Aguilera et al. (2009) represented a registration method based on a robust matching approach. Both digital images and range images were used in the matching approach. Then the matching results were put into a conventional spatial resection model to reconstruct sensor orientation using a RANSAC iteration.

2.3. Platform calibration

In current research and applications, although imagery and point cloud data could be registered together using either a direct geo-referencing method or an indirect geo-referencing method (Al-Manasir & Fraser, 2006; González-Aguilera et al., 2009), an accurate co-registration result between imagery and point cloud

data always requires an accurate relative orientation (Rönnholm et al., 2009). In the case of a mobile laser scanning platform, it means the position and altitude of digital camera should be accurately estimated with respect to geo-referenced point cloud data. Although, direct geo-referencing based on position and attitude derived from GPS/IMU system could achieve a very high accuracy, there are mainly two kinds of systematic errors in GPS/IMU integrated MLS system which may lead to an inaccurate orientation of digital camera with respect to geo-referenced laser data (Liu et al., 2011). One comes from the lever-arm offset between platform and sensors, and the other one comes from misalignment angles between the platform and digital camera. Besides errors from system mounting parameters, any error from inaccurate sensor calibration may be also directly propagated to final co-registration result. Therefore, to achieve a more accurate co-registration result between imagery and point cloud data, a system calibration procedure which includes camera calibration and system mounting parameters calibration is needed (Habib et al., 2010).

In camera calibration, the interior orientation parameters (IOP) are accurately determined. In system mounting parameters calibration, systematic errors including boresight misalignment and lever-arm offset are modelled and corrected. Several different platform calibration procedures have been developed in the past research. Generally, the mounting parameters of a hybrid multi-sensor platform, which describes the spatial relationship between sensors and platform, could be determined using either a two-step or a single step method (Jaw & Chuanga, 2010).

2.3.1.   Two-step method

The two-step procedure for system mounting parameters calibration is usually based on a comparison between platform orientation results derived from direct geo-referencing procedure and the exterior orientation parameters determined from another independent indirect geo-referencing solution (Habib et al., 2010). In this procedure, the independently estimated exterior orientation parameters and GPUS/IMU derived positions and orientations are utilized together for the estimation of lever-arm offset and boresight misalignment respectively.

In Cramer et al. (1998), a two-step procedure for the error estimation in a GPS/IMU integrated platform was developed. In this procedure, the exterior orientation parameters were first reconstructed through aerial triangulation, and then all potential errors were grouped into one error factor and corrected in an iteration procedure with a comparison between AT derived and GPS/IMU derived positions and attitudes. Grejner-Brzezinska (2001) proposed a similar two-step procedure for the estimation of boresight transformation. In this research, first, the displacement between the center of INS body frame and camera projection center were calculated. Then the level-arm offset was determined via a least-square adjustment procedure. In Casella et al. (2006), the calibration was performed based on the usual two-step procedure, and the estimation of lever-arm offset was determined by taking the arithmetic average of differences between the AT-determined exterior orientation parameters and the directly geo-referenced ones. Liu et al. (2011) also presented a two-step approach for IMU boresight misalignment calibration. In this approach, boresight misalignment was estimated based on a linearized misalignment model. As for the lever-arm offset, the writer suggested it could be corrected based on an accurate measurement on the platform.

Because any bundle adjustment software could easily reconstruct the exterior orientation parameters for system calibration, this two-step procedure (Cramer et al., 1998; Cramer & Tuttgart, 1999; Jacobsen, 1999; Skaloud, 1999; Grejner-Brzezinska, 2001; Cramer & Stallmann, 2002; Yastikli & Jacobsen, 2005; Casella et al., 2006; Liu et al., 2011) has been widely used in current research. On the other hand, the disadvantages of this procedure are also obvious. On drawback of this procedure is the final calibration quality is heavily

dependent on the quality of EOPs determined from independent indirect geo-referencing procedure (the bundle adjustment). Another one is that the selection and distribution of tie point will also influence the final result, since it will influence the accuracy of estimated EOPs.

2.3.2. Single-step method

The single-step procedure incorporates the system mounting parameters as well as GPS/IMU derived position and orientation information in a bundle adjustment procedure. Compared with the two-step procedure, the single-step procedure is much more robust to handle the discrepancies between system mounting parameters calibration and camera calibration. Because the interior orientation parameters of camera could be estimated together with system mounting parameters in the same bundle adjust procedure (Mostafa & Schwarz, 2001; Habib et al., 2010).

This single-step procedure could be carried out in two different approaches. The first approach consists of extending existing bundle adjustment procedures with constraint equations which are used for enforce the constant geometric relationship between different sensors (El-Sheimy, 1992; King, 1993; Cramer & Stallmann, 2002; Honkavaara et al., 2003; Smith et al., 2006; Lerma et al., 2010). To be more specific, the conventional bundle adjustment procedures were usually expanded by adding constraint equations which described the relative orientation between cameras and IMU body coordinate system. Although additional constraint equations guaranteed consistent relative orientation among different sensors, it associated with an increased complexity of implementing this approach.

In the second approach, system mounting parameters as well as GPS/IMU derived data are directly incorporated into the collinearity equation (Pinto & Forlani, 2002; Rau et al., 2011). Compared with the first approach, this method is much easier to implement, especially for a single camera platform. Pinto and Forlani (2002) presented a single-step procedure with a modified collinearity equations for the calibration of imu/gps integrated system. In this procedure, the calibration parameters will be directly inserted into collinearity equations, and the projection center of camera will be replaced by the sum of IMU position and lever-arm offset from IMU to the camera. Rau et al. (2011) also proposed a novel single-step procedure utilizing the concept of modified collinearity equations. In this improved procedure, the estimation of system mounting parameters was carried out based on a linearized mathematical model, and this proposed procedure also allowed for the feasibility of using the same model for GPS-assisted, GPS/INS-assisted or indirectly geo-referenced photogrammetric bundle adjustment.

2.4. Summary

Based on the review of current research, we could notice that although both the single-step procedure and two-step procedure for the platform calibration have been fully developed and widely used in various applications, most of them are based on an airborne platform. As for a mobile laser scanning platform which also integrated GPS/IMU system for direct geo-referencing, little work has been done on the platform calibration part.

In the meantime, for a system calibration procedure of a mobile platform, usually a test field and several control points or surveyed targets are needed (Rau et al., 2011). The configuration of the test field and arrangements of control points also need a strict control to guarantee an accurate calibration result. The

whole procedure is time consuming and expensive, and usually not available to the end users who only focus on the use of data.

Therefore, there is a need to improve existing methods or develop a new method for current mobile laser scanning platform. In this research, the proposed procedure will focus on platform bias modelling and correction. No test field or ground control points are needed in this research. Finally, the co-registration quality between imagery and point cloud data acquired by the same MLS platform is also expected to be improved via this procedure.

3. PROPOSED METHOD

3.1. Overview

To properly register both imagery and point cloud data into one common coordinate system, the geometric relationship between digital camera and the geo-referenced point cloud data must be recovered. In direct geo-referencing procedure, this relationship can be established directly based on the position and attitude information derived from GPS/IMU data. However, mainly due to the inaccurate system mounting parameters, the attitudes and positions of each sensor are usually badly estimated. Therefore, in this research, a two-step calibration procedure is developed. The aim of this procedure is to find the potential error sources that may influence the co-registration quality between imagery and point cloud data acquired by the same MLS system. An overview of the proposed procedure is illustrated in Figure 3.1.

Point clouds data and imagery acquired by MLS platform

↓

Camera Calibration (model and correct radial distortion)

↓

Recover the orientation of image in a local coordinate system

↓

Registration from image to the point cloud data via 3-D similarity transformation

↓

Reconstruct the exterior orientation parameters of the camera with respect to the geo-referenced point cloud data

↓

Estimate and determine the bias caused by inaccurate platform orientation

↓

Correct bias and improve co-registration quality

↓

Evaluate co-registration quality after correction

Figure 3.1 Methodology adapted

In the first step of this proposed procedure, an indirect co-registration method is developed to estimate the orientation of the camera with respect to the geo-referenced point cloud data. The mathematical model used for camera calibration is presented in Section 3.2. Then, the feature-based co-registration method, which includes point, line and plane features, is presented in Section 3.3.

Based on the proposed method in the first step, the exterior orientation parameters of the camera can be reconstructed. In the second step of this proposed procedure, the reconstructed exterior orientation parameters are compared with the original exterior orientation parameters which are derived from GPS/IMU recordings. From the comparison, we can then estimate the bias on system mounting parameters of the MLS platform. The established mathematical model for bias estimation on boresight angles and lever-arm offsets is introduced in Section 3.4.

3.2.   Camera Calibration

Real lenses usually have two types of distortions, radial distortion and tangential distortion. In photogrammetry, these distortions usually lead to a significant impact on image geometry and will directly influence the final co-registration result between imagery and point cloud data.

Radial distortion is associated with any lens and particularly visible when taking pictures of vertical structures having straight lines. Due to the influence of radial distortion, straight lines or other regular structures in the world are often distorted and curved when they are projected onto images. There are two types of radial distortion, barrel distortion and pincushion distortion. The visible effect of barrel distortion is that lines that not through the center of the image are bowed outwards from the center of the image, whereas the effect of pincushion distortion is just opposite. Lines in pincushion distorted images are bowed inwards, towards the center of the image.
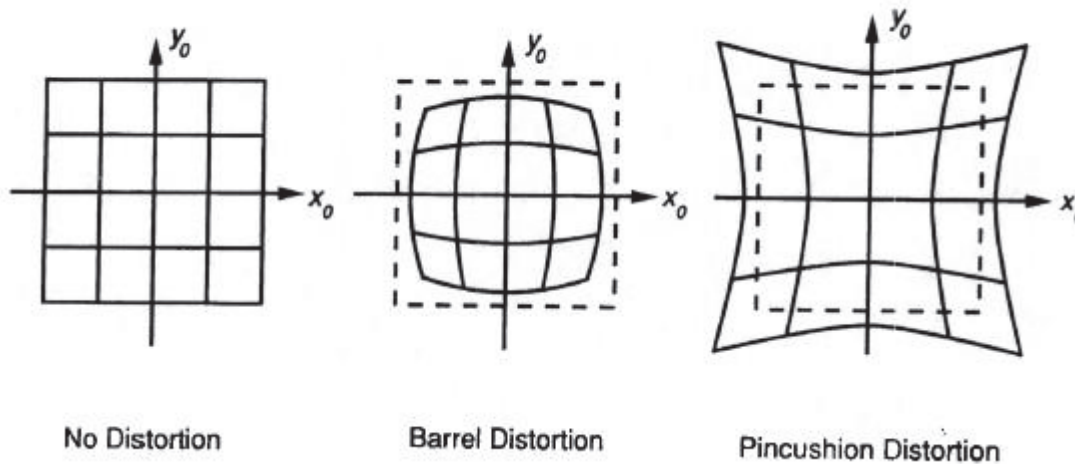
Figure 3.2 Effect of radial distortion on image geometry (Cologne, 2012)

Compared with radial distortion, tangential distortion also known as decentering distortion usually only has slight effects on image geometry. Therefore, in general, only radial distortion is considered into distortion correction.

The purpose of camera calibration is to recover the interior orientation parameters of a camera. The camera calibration model considering the effects of radial distortion could be given based on an extended collinearity equation (Fraser, 1997).

$$\begin{cases} x - x_0 + \Delta x = -c\dfrac{r_{11}(X - X_0) + r_{21}(Y - Y_0) + r_{31}(Z - Z_0)}{r_{13}(X - X_0) + r_{23}(Y - Y_0) + r_{33}(Z - Z_0)} \\[2ex] y - y_0 + \Delta y = -c\dfrac{r_{12}(X - X_0) + r_{22}(Y - Y_0) + r_{32}(Z - Z_0)}{r_{13}(X - X_0) + r_{23}(Y - Y_0) + r_{33}(Z - Z_0)} \end{cases}$$

Equation 3-1

Where:

$$\Delta x = (x - x_0)(K_1 r^2 + K_2 r^4 + K_3 r^6)$$
$$\Delta y = (y - y_0)(K_1 r^2 + K_2 r^4 + K_3 r^6)$$
$$r = \sqrt{(x - x_0)^2 + (y - y_0)^2}$$

Equation 3-2

In this equation, x and y are distorted image coordinates, and Δx and Δy are the correction for radial distortion; x_0 and y_0 are the coordinates of principal point which is usually at the center of image; K_1, K_2 and K_3 are radial distortion coefficients. This mathematical model is widely used for digital camera self-calibration and can be solved in a bundle adjustment procedure (Fraser, 1997).

3.3. Feature-based co-registration between imagery and point cloud

In general, to properly orient one image in the local mapping coordinate system, the interior orientation parameters and the exterior orientation parameters of the camera at the exposure moment need to be given. In previous section, the method and the mathematical model for camera calibration has been introduced. In this section, the proposed feature-based co-registration method is presented. Based on this method, the exterior orientation parameters of the camera can be reconstructed.

3.3.1. Relationship between digital camera and geo-referenced point cloud

In this research, the exterior orientation parameters of the camera are determined with a relative-absolute orientation.

First, a step of relative orientation is needed. In this proposed method, the relative orientation is performed by a free network adjustment. With this procedure, overlapped images acquired by the MLS platform can be relatively oriented and adjusted in a photogrammetric network. Then, the orientation of each image can be reconstructed in a local coordinate system. Meanwhile, considering the MLS platform may take images on different driving directions, to eliminate the correlations on different driving directions, four strips of images acquired on different driving directions are needed in this research. For each image strip, the free network adjustment will perform separately.

After the relative orientation step, the coordinates of the selected tie points in the photogrammetric network can be also recovered in the local coordinate system. Therefore, a 3D to 3D similarity transformation can be applied to determine the transformation from the local coordinate system to the mapping coordinate system. Using the same transformation parameters, the positions and attitudes (EOPs) of the camera can be reconstructed in the mapping coordinate system as well.

In general, the 3D similarity transformation is carried out with corresponding point features. However, due to the property of point cloud data, it's usually very hard to have an accurate point-to-point match

between the relatively oriented image network and the point cloud data. In this research, considering lines and planes are also the most common geometric features in survey, especially in the survey of urban areas, line features and plane features will be also used to solve the 7 parameters in the proposed 3D similarity transformation (Jaw & Chuanga, 2010).

From Section 3.3.2, the point-based, line-based and plane-based similarity transformation will be introduced respectively. Then a multi-feature based strategy will be presented in Section 3.3.5.

3.3.2. Point-based similarity transformation

The 3D similarity transformation of two Cartesian coordinate systems could be established based on a point-to-point correspondence. In this case, the 3D similarity transformation is applied to transform points from recovered local coordinate system of camera to the mapping coordinate system. The point-based formula is given as Equation 3-3.

$$\begin{bmatrix} X_i \\ Y_i \\ Z_i \end{bmatrix} = s \cdot R \cdot \begin{bmatrix} x_i \\ y_i \\ z_i \end{bmatrix} + \begin{bmatrix} T_x \\ T_y \\ T_y \end{bmatrix} \qquad \text{Equation 3-3}$$

Where:
(x_i, y_i, z_i) is the ith point in the recovered local coordinate system of camera;
(X_i, Y_i, Z_i) is the correspondent ith point in geo-referenced point cloud data given in mapping coordinate system;
s is the scale factor;
R is the rotation matrix relating local coordinate system of camera to the mapping coordinate system; this rotation matrix could be given as Equation 2-2;
$[T_x, T_y, T_z]$ is the translation vector between two coordinate systems.

To solve this equation, at least 3 pairs of non-collinear points are needed. In this research, potential conjugate point features must be identifiable in at least two images, so that the 3D coordinates of selected points could be adjusted and recovered in the photogrammetric network. Likewise, these point features must be measurable in the point cloud data as well.

3.3.3. Line-based similarity transformation

Due to the properties of point cloud data, it's usually very hard to find accurate point-to-point matches in both imagery and point cloud data. On the other hand, line features (line segments) are very common and easy to detect from man-made objects. Therefore, correspondent line features could be a potential alternative for the point-to-point based 3D similarity transformation. A optimal four-parameter (a, b, p, q) representation of 3D lines is preferred in current research (Ayache & Faugeras, 1989). In this representation method, a line (not perpendicular to the z axis) could be considered as the intersection of two planes parallel to x axis and y axis respectively (See Figure 3.3). The equation for this representation is given in Equation 3-4.

$$\begin{cases} x = p + az \\ y = q + bz \end{cases}$$

Equation 3-4

Where:

$[a, b, 1]$ is the direction vector of the line;

$(p, q, 0)$ is the point of intersection of the line with the xy plane.
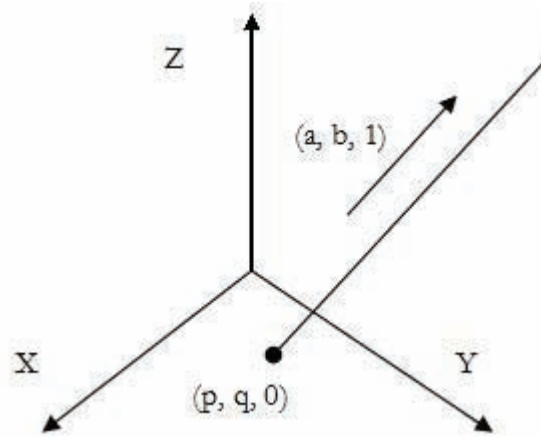
Figure 3.3 4-parameter representation of 3D line

However, this representation can't be used for line perpendicular to z axis or parallel to xy plane. To solve this problem, another representation must be applied. For example:

$$\begin{cases} y = p + ax \\ z = q + bx \end{cases}$$

Equation 3-5

which could represent lines not perpendicular to x axis or parallel to yz plane, or

$$\begin{cases} z = p + ay \\ x = q + by \end{cases}$$

Equation 3-6

which could represent lines not perpendicular to y axis or parallel to xz plane.
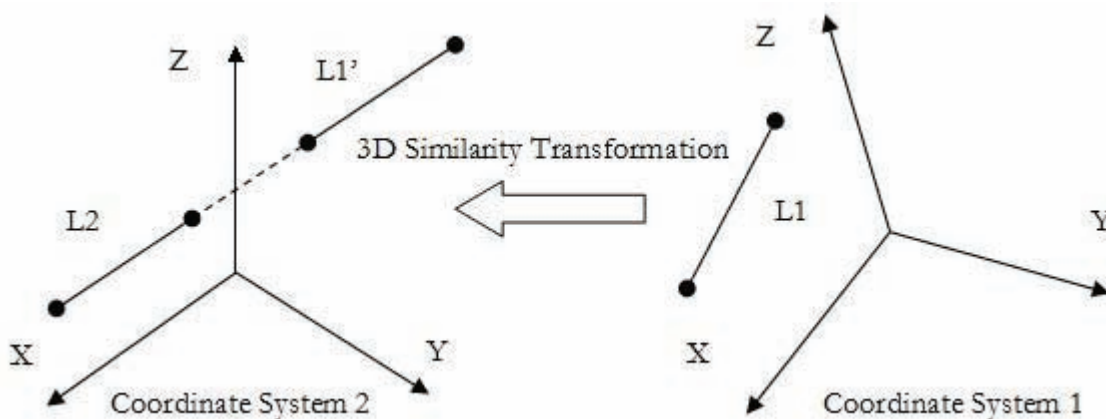
Figure 3.4 Collinearity relationship of corresponding line features after 3D similarity transformation

Just as Figure 3.4 illustrates, after a 3D similarity transformation, transformed line feature L1' from coordinate system 1 should be collinear with its corresponding line feature L2 in coordinate system 2. In the meantime, this also indicates that any point on L1 should be collinear with L2 after applying the same

transformation. Therefore, the 3D similarity transformation of the corresponding line features could be established as Equation 3-7. The above mentioned representation method of 3D line is used in this equation.

$$\begin{cases} x' = p + az' \\ y' = q + bz' \end{cases}$$

<div align="right">Equation 3-7</div>

Where:

(x', y', z') is the coordinates of transformed point on L1' given in coordinate system 2; (x', y', z') is calculated in Equation 3-3 based on the point-to-point 3D similarity transformation;

p, q, a and b are the 4 representation parameters of L2, Here, we assume L2 is not perpendicular to z axis. If L2 is perpendicular to z axis or parallel to xy plane, representation methods in Equation 3-5 and Equation 3-6 should be used.

In this line feature based method, a pair of corresponding line features could create 4 equations (two equations for each endpoint). Therefore, at least 2 pairs of 3D line features (not on the same plane) are needed to solve seven parameters in the 3D similarity transformation. In this research, the 3D coordinates of points on line features extracted from images could be recovered in a local coordinate system. The 3D lines in point clouds data could be calculated based on the intersection of two adjacent planes (see Figure 3.5). So the point (from imagery) to line (in point cloud data) strategy could be applied based on above mentioned mathematical model in Equation 3-7.

<div align="center">(a)   (b)</div>
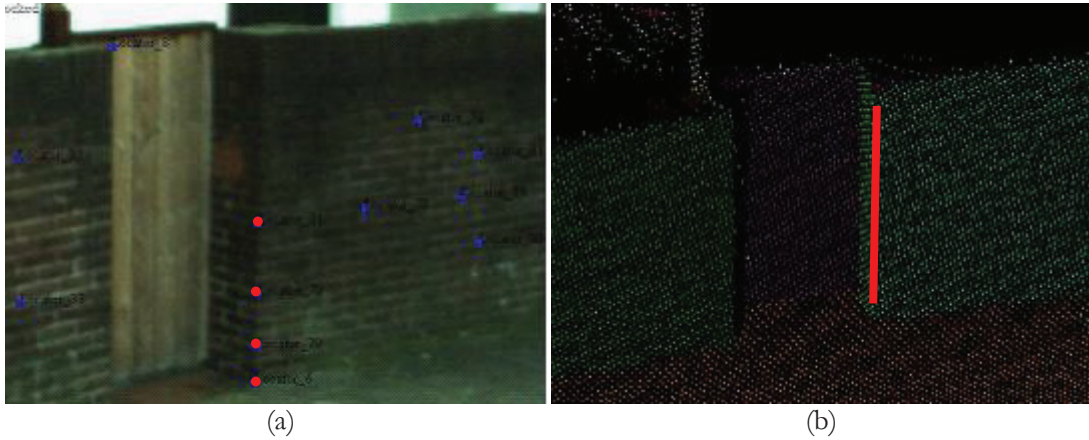
Figure 3.5 (a) points on line feature in image (specified by the red points on the edge of the wall); (b) 3d line feature in laser data (intersection of two adjacent planes, specified by the red line)

3.3.4. Plane-based similarity transformation

A plane is another common feature on man-made objects, and plane features are much easier to be detected and segmented in point cloud data. Therefore, a plane-based similarity transformation is considered in this research. A common way to define a 3D plane is to specify one point on this plane and a normal vector to this plane. This representation method is given as:

$$n_x(x - x_0) + n_y(y - y_0) + n_z(z - z_0) = 0$$

<div align="right">Equation 3-8</div>

Where:

$[n_x, n_y, n_z]$ is the normal vector of this plane and (x_0, y_0, z_0) is the given point on this plane. Usually this equation could be changed into a plane equation with 4 parameters, where d is the distance from the plane to the origin of the coordinate system.

$$n_x \cdot x + n_y \cdot y + n_z \cdot z - d = 0 \qquad \text{Equation 3-9}$$

Because after applying the 3D similarity transformation, all points from one plane feature will fall onto its corresponding plane in another data set, the plane-based transformation could be established by simply substituting (x, y, z) in the plane equation with the coordinates of transformed points from its corresponding plane. The equation is given as:

$$[n_x, n_y, n_z] \cdot \left(s \cdot R \cdot \begin{bmatrix} x \\ y \\ z \end{bmatrix} + T \right) - d = 0 \qquad \text{Equation 3-10}$$

In this method, at least three points are needed for each plane, and at least four intersecting planes are needed to solve all the 7 transformation parameter (Jaw & Chuang, 2008). Among these four intersecting planes, at most two planes can be parallel. Meanwhile, because one 3D line or one 3D point could be represented by the intersection of two planes or three planes respectively, the point-based and line-based methods could be extended to the plane-based method as well. In this extended plane-based method, one point on a 3D line can establish two equations (one equation for one corresponding plane), while one 3D point can establish three equations. Compared with point features and line features, planes could be more accurately estimated in the point cloud data, because there are usually thousands of point measurements on each plane. Therefore, this extended plane-based method could provide a much more accurate estimation of transformation parameters. A summary of point, line and plane-based similarity transformation is given in Table 3-1.

Table 3-1 Summary of three different feature-based similarity transformation methods

Method	Measurement of Correspondence	Minimal Number of Correspondence	Number of Equations for Each Correspondence
Point Based	3 coordinates for each corresponding point	at least 3 pairs of corresponding non-collinear points	3 functions for each pair of corresponding points
Line Based	at least two points on one 3D line, and 4 parameters for corresponding 3D line	at least 2 pairs of corresponding non-intersecting lines (two lines not on the same plane)	4 Equations for each pair of corresponding lines (2 equations for each point)
Plane Based	at least 3 points on one plane, and 4 parameters for corresponding plane	at least 4 pairs of corresponding planes (at most two planes may be parallel)	3 Equations for each pair of corresponding planes (1 equation for each point)

3.3.5. Multi-feature based similarity transformation

Based on above analysis, a multi-feature based strategy is developed for the co-registration between imagery and point cloud data. This strategy consists of two main steps. In the first step, several corresponding point features are extracted from both images and point cloud data. Then a point-based

method is applied to obtain an approximate estimation of transformation parameters between these two different coordinate systems. In the second step, an extended plane-based method is used to refine the result. Estimated transformation parameters derived from point-based method are used as the initial values in this step. The basic workflow is illustrated in Figure 3.6.
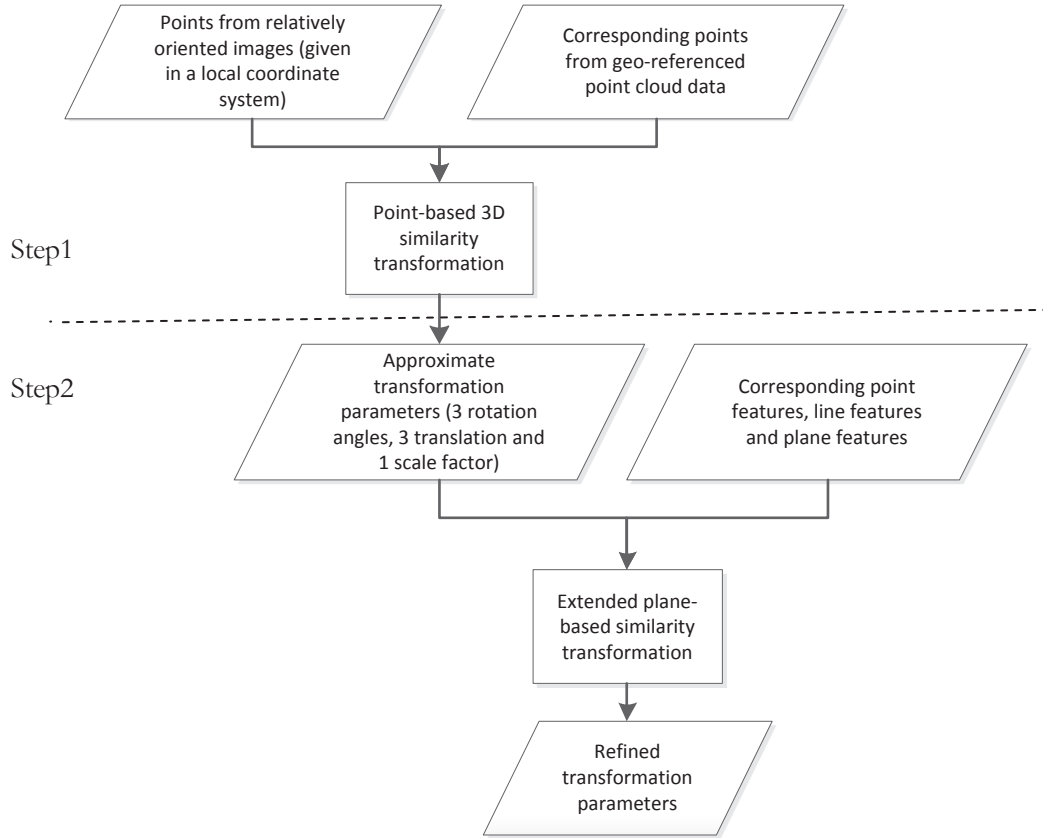
Figure 3.6 Basic workflow of multi-feature based co-registration in this research

3.3.6. Calculate the exterior orientation parameters of camera

Based on the same similarity transformation parameters derived from multi-feature based transformation, the position and attitude of camera in the local coordinate system could be transformed into the mapping coordinate system. Equation 3-11 illustrates how to recovery the position and attitude of camera in the mapping coordinate system.

$$\begin{cases} \begin{bmatrix} X \\ Y \\ Z \end{bmatrix} = s \cdot R \cdot \begin{bmatrix} x \\ y \\ z \end{bmatrix} + T \\ R_{mapping} = R \cdot R_{local} \end{cases}$$

Equation 3-11

Where:

x, y and z are the coordinates of camera perspective center in the local coordinate system;

X, Y and Z are the coordinates of camera perspective center in the mapping coordinate system;

s, R and T are the scale factor, rotation matrix and translation vector relating the local coordinate system to the mapping coordinate system; these parameters are derived from the proposed multi-feature based co-registration method;

R_{local} is the rotation matrix from camera coordinate system to the local coordinate system;

$R_{mapping}$ is the rotation matrix from camera coordinate system to the local coordinate system.

For each image, the exterior orientation parameters can be recovered through Equation 3-11. Then the geo-referenced point cloud data and images can be registered together through the conventional collinearity equations.

3.4. Bias estimation of MLS platform

Although both digital cameras and laser scanner are rigidly fixed on the same mobile platform, inaccurately estimated platform mounting parameters still affect the quality of co-registration between imagery and point cloud data. In Chapter 3.3, a multi-feature based co-registration method has been introduced. By using this method, the exterior orientation parameters of images can be reconstructed. In this section, both the reconstructed EOPs (determined from the multi-feature based co-registration) and the original EOPs (derived from direct geo-referencing) of the same camera will be utilized together for the estimation of bias on the camera's system mounting parameters. Because system mounting parameters of the camera in an MLS platform usually consists of the boresight angles and the lever-arm offset, the estimated bias on different system parameters will be discussed and presented separately. The mathematical model for the estimation of bias on boresight angles is introduced and presented in Section 3.4.1, and the model for lever-arm offset is presented in Section 3.4.2.

3.4.1. Bias modelling for boresight angles

In a mobile laser scanning platform integrated GPS/IMU system, the boresight angles describe the rotation from camera frame to the IMU body frame. Because the axes of IMU are usually invisible, the boresight angles can be only determined in an indirect way (estimated in system calibration). If the boresight angles are not accurately estimated in the system calibration, the geometric relationship between camera and geo-referenced point cloud data may be very poorly recovered, and the co-registration quality may be affected as well.

Figure 3.7 illustrates the geometric relationship among different sensors and IMU body frame in the same mobile laser scanning platform. The rotation from the camera body coordinate system to the mapping coordinate system could be established as Equation 3-12.

$$R = R_{P\_M}(t) \cdot R_{Boresight} \qquad \text{Equation 3-12}$$

Where:
R: is the rotation matrix relating the camera body coordinate system to the mapping coordinate system defined by $(\omega, \varphi, \kappa)$;

$R_{P\_M}(t)$ is the rotation matrix relating the IMU body frame (derived through the GPS/INS integration process) to the mapping coordinate system at time (t);

$R_{Boresight}$ is the rotation matrix relating the camera body coordinate system to the IMU body frame, defined by three boresight angles.
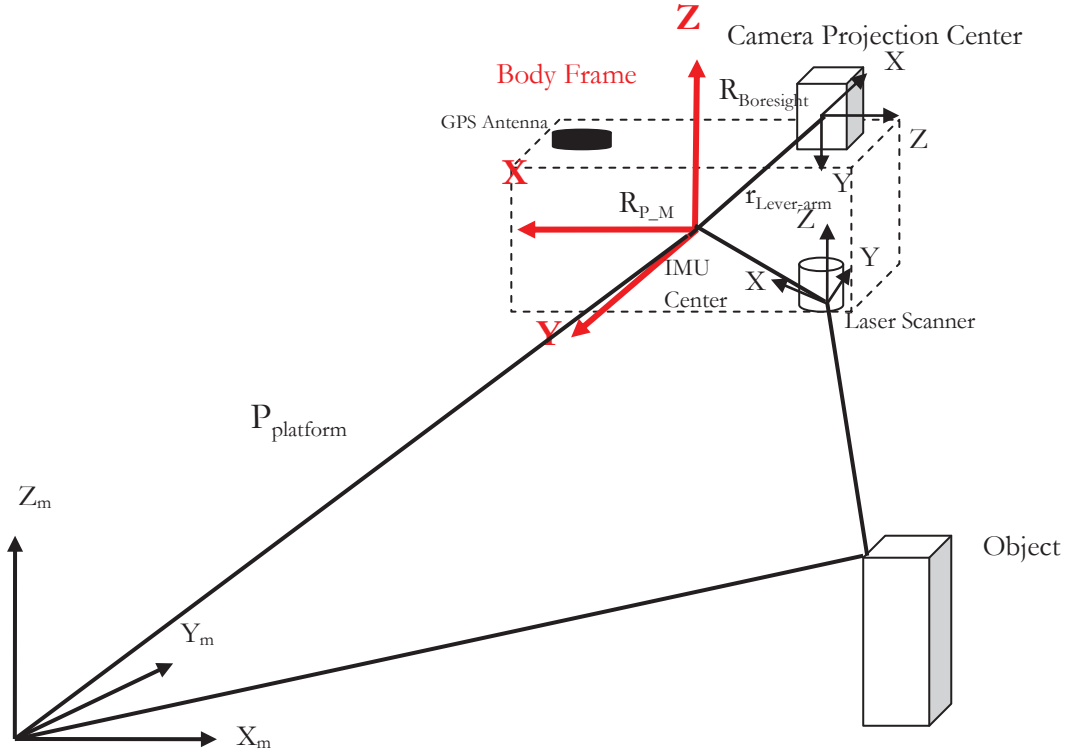
Figure 3.7 Simplified relationship of Mobile Laser Scanning platform

However, due to the inaccurate estimated boresight angles, after transformation, the axes of IMU platform and the axes of camera usually can't perfectly coincide with each other. There are small angle offsets between corresponding axis pairs. The aim of bias modelling on boresight angles is to estimate these small angle offsets.

$$R_{estimated} = R_{original} \cdot R_{corretion}(\alpha, \beta, \gamma)$$

<div align="right">Equation 3-13</div>

Equation 3-13 is the mathematical model for bias estimation on boresight angles. In this equation, $R_{estimated}$ is the rotation matrix of estimated exterior orientation parameters which derived from above mentioned multi-feature based co-registration method; $R_{original}$ is the rotation matrix of original exterior orientation parameters which derived from direct geo-referencing; $R_{corretion}(\alpha, \beta, \gamma)$ is the corrected rotation matrix, and (α, β, γ) are the three angle offsets on three axes. To solve this equation, Equation 3-13 can be changed into:

$$R_{corretion}(\alpha, \beta, \gamma) = R_{original}^{T} \cdot R_{estimated} = \begin{bmatrix} r_{11} & r_{12} & r_{13} \\ r_{21} & r_{22} & r_{23} \\ r_{31} & r_{32} & r_{33} \end{bmatrix}$$

<div align="right">Equation 3-14</div>

Where:

$$\begin{cases} r_{11} = \cos\beta\cos\gamma \\ r_{12} = \sin\alpha\sin\beta\sin\gamma - \cos\alpha\sin\gamma \\ r_{13} = \cos\alpha\sin\beta\cos\gamma + \sin\alpha\sin\gamma \\ r_{21} = \cos\beta\sin\gamma \\ r_{22} = \sin\alpha\sin\beta\sin\gamma + \cos\alpha\cos\gamma \\ r_{23} = \cos\alpha\sin\beta\sin\gamma - \sin\alpha\cos\gamma \\ r_{31} = -\sin\beta \\ r_{32} = \sin\alpha\cos\beta \\ r_{33} = \cos\alpha\cos\beta \end{cases}$$

Equation 3-15

This is an equation system with nine non-linear equations and can't be solved directly. In general, the unknown parameters are obtained by successive approximation in the non-linear least squares adjustment. Equation 3-15 is the linearized equation by approximation to a first-order Taylor series expansion. The estimated parameters are refined iteratively based on this linearized equation system.

$$F = \begin{bmatrix} r_{11} - f_1(\alpha^k, \beta^k, k^k) \\ \vdots \\ r_{33} - f_9(\alpha^k, \beta^k, k^k) \end{bmatrix} = J \cdot \begin{bmatrix} \Delta\alpha \\ \Delta\beta \\ \Delta\gamma \end{bmatrix} + \varepsilon$$

Equation 3-16

Where:

(α^k, β^k, k^k) is the approximation values of α, β and γ at the kth iteration;

$$J = \begin{bmatrix} \frac{\partial f_1}{\partial\alpha} & \frac{\partial f_1}{\partial\beta} & \frac{\partial f_1}{\partial\gamma} \\ \vdots & \vdots & \vdots \\ \frac{\partial f_9}{\partial\alpha} & \frac{\partial f_9}{\partial\beta} & \frac{\partial f_9}{\partial\gamma} \end{bmatrix}$$ is the Jacobian Matrix;

$\begin{bmatrix} \Delta\alpha \\ \Delta\beta \\ \Delta\gamma \end{bmatrix}$ is the correction vector to the approximate values of α, β and γ;

For n observations (n images), each image can establish 9 linearized equations, and the correction vector to the approximate values can be calculated as:

$$\begin{bmatrix} \Delta\alpha \\ \Delta\beta \\ \Delta\gamma \end{bmatrix} = \left(\sum_{i=1}^{n} (J_i^T \cdot J_i) \right)^{-1} \cdot \left(\sum_{i=1}^{n} (J_i^T \cdot F_i) \right)$$

Equation 3-17

The iteration doesn't stop until the correction vector smaller than the tolerance. In this research, the initial values of estimated parameters can be all set to zero. The problem for this method is the creation of Jacobian Matrix is time-consuming.

As an alternative for the non-linear least squares adjustment, Bäumker and Heimes (2001) proposed a simplified method to solve these three boresight misalignment angles. In this method, the authors assumed that all three angles are very small, so the rotation matrix can be expressed as a differential rotation matrix:

$$R_{correction} = \begin{bmatrix} 1 & -\gamma & \beta \\ \gamma & 1 & -\alpha \\ \beta & \alpha & 1 \end{bmatrix}$$

Equation 3-18

Then, the nine equations can be changed into a linear equation system, and the three angles can be solved directly based on the linear least squares adjustment procedure. By substituting $R_{correction}(\alpha, \beta, \gamma)$ with this differential rotation matrix, the 9 nonlinear equations can be rewritten as:

$$y = Ax + \varepsilon$$

<div align="right">Equation 3-19</div>

Where:

$$y = \begin{bmatrix} r_{11} \\ r_{12} \\ r_{13} \\ r_{21} \\ r_{22} \\ r_{23} \\ r_{31} \\ r_{32} \\ r_{33} \end{bmatrix} - \begin{bmatrix} 1 \\ 0 \\ 0 \\ 0 \\ 1 \\ 0 \\ 0 \\ 0 \\ 1 \end{bmatrix} \quad And \quad A = \begin{bmatrix} 0 & 0 & 0 \\ 0 & 0 & -1 \\ 0 & 1 & 0 \\ 0 & 0 & 1 \\ 0 & 0 & 0 \\ -1 & 0 & 0 \\ 0 & 1 & 0 \\ 1 & 0 & 0 \\ 0 & 0 & 0 \end{bmatrix} \quad And \quad x = \begin{bmatrix} \alpha \\ \beta \\ \gamma \end{bmatrix}$$

ε is the vector of residuals.

After applying this equation to each image, the estimated bias on lever-arm offset could be solved in least squares adjustment:

$$\hat{x} = \left(\sum_{i=1}^{n} (A_i^T \cdot A_i) \right)^{-1} \cdot \left(\sum_{i=1}^{n} (A_i^T \cdot y_i) \right)$$

<div align="right">Equation 3-20</div>

Where:

n is the total number of images used for bias estimation.

Based on the error propagation law, the covariance matrix of three estimated parameters (α, β, γ) can be calculated as:

$$C_x = D \cdot C_y \cdot D^T$$

<div align="right">Equation 3-21</div>

Where:

$D = (A^T \cdot A)^{-1} \cdot A^T$, and C_y is the covariance matrix of residuals.

This alternative linear method only holds when the three estimated angles are very small. In this research, because all the three estimated angle offsets are very small angles, both this linear method and the non-linear least squares adjustment give similar estimation. Considering the efficiency of the linear method, in the experimental test, the linear method is used for the estimation of bias on the boresight angles.

3.4.2. Bias Modelling for lever-arm offset

Lever-arm offset describes the translation vector from IMU body frame to the camera projection center. Just as Figure 3.7 illustrates, the position of camera projection center in the mapping coordinate system could be given as:

$$T = P_{platform}(t) + R_{P\_M}(t) \cdot r_{level\_arm}$$

<div align="right">Equation 3-22</div>

Where:

T: is the position of the camera projection center in mapping coordinate system;

$P_{platform}(t)$ is the position of the origin of IMU body frame at given time (t) when the camera captured a image;

r_{level_arm} is the level-arm offset defined by a vector [X, Y, Z] between the origin of IMU body frame and the camera projection center; it is given in the body frame coordinate system;

To model the errors from inaccurate lever-arm offset, Equation 3-22 can be rewritten as:

$$T_{estimate} = P_{platform}(t) + R_{P_M}(t) \cdot (r_{lever\_arm} + \begin{bmatrix} \Delta x \\ \Delta y \\ \Delta z \end{bmatrix}) \qquad \text{Equation 3-23}$$

In this equation, $\Delta x, \Delta y$ and Δz are the estimated errors on lever-arm offset. This equation could be simplified a step further as:

$$T_{estimate} - T = R_{P_M}(t) \cdot \begin{bmatrix} \Delta x \\ \Delta y \\ \Delta z \end{bmatrix} \qquad \text{Equation 3-24}$$

Because this is a linear equation system, it can be also rewritten as the form of:

$$y = Ax + \varepsilon \qquad \text{Equation 3-25}$$

After applying this equation to each image, the estimated bias on lever-arm offset can be solved as Equation 3-20, and the covariance matrix for estimated parameters can be calculated as Equation 3-21.

3.4.3. Co-registration after bias correction

In previous sections, the mathematical models of bias on boresight angles and lever-arm offsets have been introduced. In this research, both estimated bias can be solved in the least squares adjustment procedure. With the estimated bias, the original exterior orientation parameters of camera can be corrected in the post-processing procedure. Then, co-registration between imagery and point cloud data can be improved based on corrected exterior orientation parameters. Equation 3-26 illustrates the mathematical model of co-registration. Both radial distortion correction and platform bias correction are considered in this model.

$$\begin{bmatrix} X \\ Y \\ Z \end{bmatrix} = P_{platform}(t) + R_{P\_M}(t) \cdot (r_{lever\_arm} + \begin{bmatrix} \Delta x \\ \Delta y \\ \Delta z \end{bmatrix}) + R_{P\_M}(t) \cdot R_{Boresight} \cdot R_{corretion}(\alpha, \beta, \gamma) \cdot \lambda \cdot x$$

$$\text{Equation 3-26}$$

Where:

$x = \begin{bmatrix} x - x_0 + \Delta x \\ y - y_0 + \Delta y \\ -c \end{bmatrix}$ is the coordinates of image point in the camera coordinate system;

λ is the scale factor, which is the ratio between the objector vector(the vector from the camera projection center to the object point) and the image vector(the vector from the camera projection center to the image point); the scale factor can be eliminated when this equation modified as the form of collinearity equations.

This equation can be also modified as the form of collinearity equations, and then the geo-referenced laser points can be transformed from the object space to the image space.

$$\begin{cases} x - x_0 + \Delta x = -c \dfrac{r_{11}(X - T_x) + r_{21}(Y - T_y) + r_{31}(Z - T_z)}{r_{13}(X - T_x) + r_{23}(Y - T_y) + r_{33}(Z - T_z)} \\[2ex] y - y_0 + \Delta y = -c \dfrac{r_{12}(X - X_0) + r_{22}(Y - Y_0) + r_{32}(Z - Z_0)}{r_{13}(X - T_x) + r_{23}(Y - T_y) + r_{33}(Z - T_z)} \end{cases} \qquad \text{Equation 3-27}$$

In this equation, the rotation matrix is from the local mapping coordinate system to the camera coordinate system, and the translation vector is the position of the camera projection center at each exposure moment.

3.5.   Summary

A whole workflow of the proposed method in this research is illustrated in Figure 3.8.
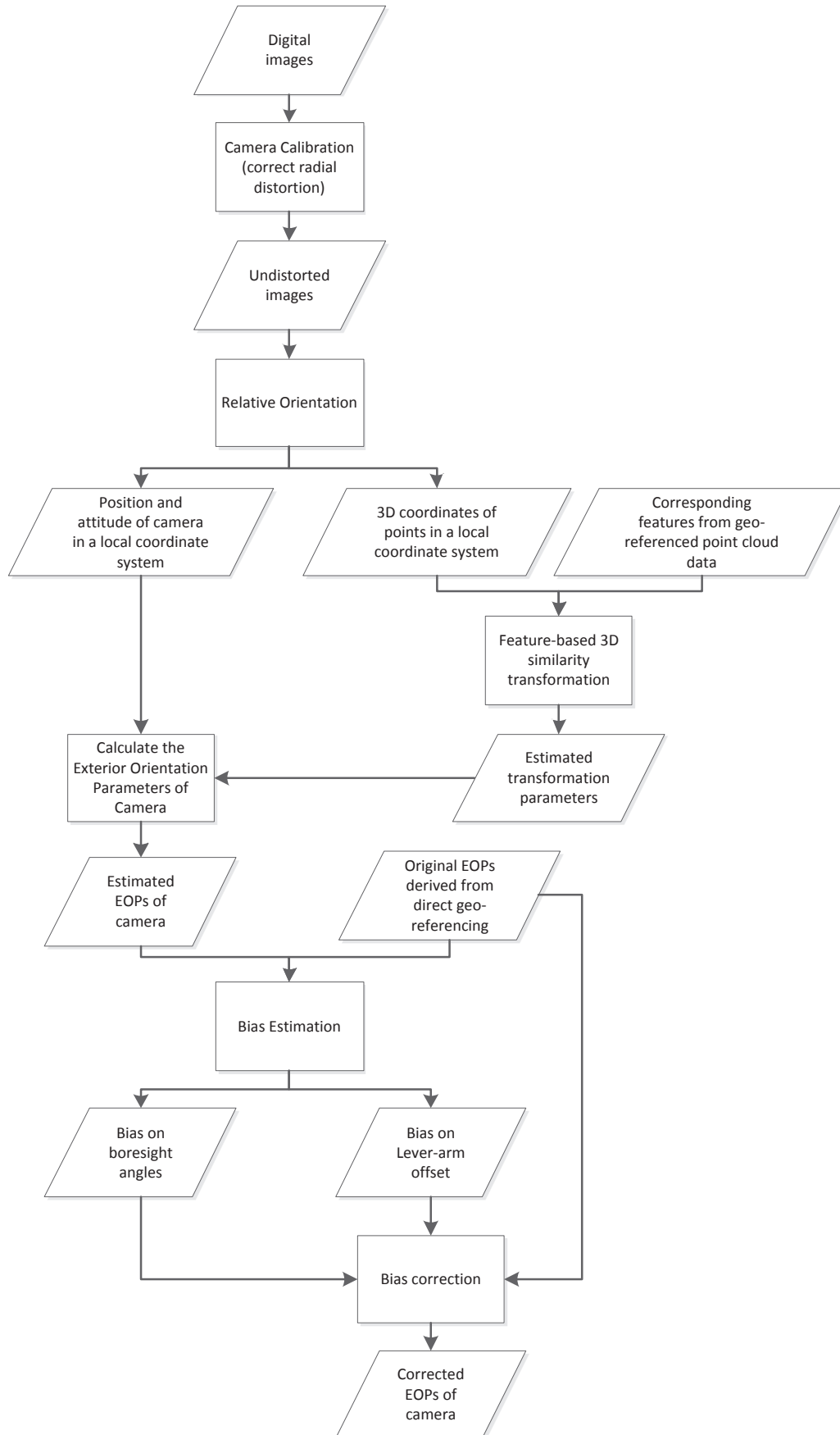
Figure 3.8 The workflow of proposed method

4.   RESULTS AND ANALYSIS

4.1.   Description of experimental data

The test site is located in Enschede, Netherlands. The point cloud data and imagery were acquired by the same MLS platform (Optech's LYNX system). This mobile laser scanning system incorporates two digital cameras and two rotating laser scanners. Both the cameras and the laser scanners are rigidly mounted on the back of the platform, and each is oriented at a 45 degrees angle with driving direction of the vehicle. Imagery and point cloud data were simultaneously acquired by this MLS platform. The laser measurement frequency of each scanner was 100 KHz, and the resolution of each scanner was up to 1 cm (Optech, 2012). In the test site, both driving directions were scanned and photographed.
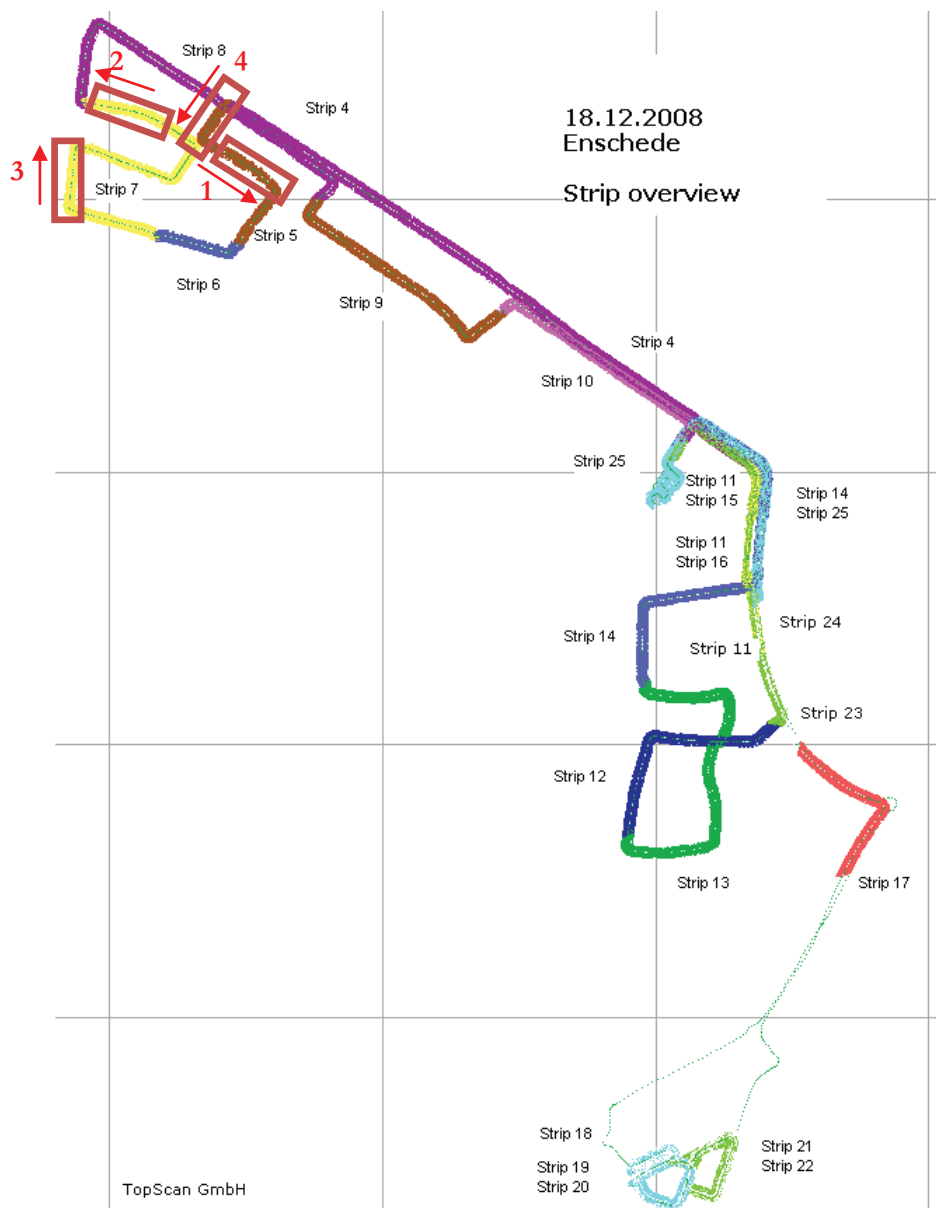
Figure 4.1 The overview of scanning strips and the approximate locations of selected image data sets; the red arrow indicates the driving direction in each selected strip

The experimental data was acquired in Enschede on December 18th, 2008. The data (both imagery and point cloud data) was carried out in 25 strips. Although this MLS platform incorporates two digital cameras (Camera 1 and Camera 2), this proposed procedure is only tested on Camera 1. For Camera 2, the implementation of this proposed procedure should be the same.

Four small blocks of images acquired on different driving directions (captured by Camera 1) are selected for testing this proposed procedure. Block 1 and Block 2 are on the east-west direction, and Block 3 and Block 4 are on the south-north direction. Each image block contains 10 overlapped images. Meanwhile, the selected geo-referenced point cloud data also covers the same area. The overview of the strips and the approximate location of the selected image block is illustrated in Figure 4.1.

4.2.   Pre-processing of experimental data

The LYNX system used in this research provided the positions and attitudes of platform derived from GPS/IMU data. Because both the coordinates of camera projection center and geo-referenced point cloud data are given in WGS 84 system, the positions of camera derived from direct geo-referencing can be directly used in the collinearity equation for the co-registration between imagery and point cloud data. However, due to the different orientation of the coordinate axes in the camera, the navigation and the mapping coordinate system, another two transformation matrices are needed to get equivalently oriented systems (Bäumker & Heimes, 2001).

1. Matrix to convert the coordinate axes from the camera coordinate system to the body frame coordinate system: R_{B_C}
2. Matrix to convert the coordinate axes from the navigation coordinate system to the mapping coordinate system: R_{M_N}

In the LYNX system, the origin of the body frame is located in the IMU system. It is defined as a right-handed coordinate system. X is pointing into the driving direction, Y to the co-driver and Z down.

Figure 4.2 The body frame coordinate system of LYNX system

As for the camera coordinate system in the LYNX system, the width of the CCD is always associated with the X axis, and the height of the CCD is always associated with the Y axis. The Z axis is perpendicular to

the image plane and pointing out the screen. So the two additional transformations needed for LYNX system are given as:

$$R_{B\_C} = \begin{bmatrix} 0 & 0 & -1 \\ 1 & 0 & 0 \\ 0 & -1 & 0 \end{bmatrix} \qquad \text{Equation 4-1}$$

$$R_{M\_N} = \begin{bmatrix} 0 & 1 & 0 \\ 1 & 0 & 0 \\ 0 & 0 & -1 \end{bmatrix} \qquad \text{Equation 4-2}$$

The final rotation matrix from the camera coordinate system to the mapping coordinate system can be given as:

$$R = R_{M\_N} \cdot R_{N\_B}(\phi, \theta, \psi) \cdot R_{B\_C} \qquad \text{Equation 4-3}$$

Where:

$R_{N\_B}(\phi, \theta, \psi)$ is the rotation matrix from body frame coordinate system to the navigation coordinate system; (ϕ, θ, ψ) are the three rotation angles given as roll, pitch and heading in the navigation coordinate system; These three angles are provided by the LYNX platform derived from GPS/IMU data.

For the conventional collinearity equation used for the co-registration, the rotation matrix is from the mapping coordinate system to the camera coordinate system. So to achieve this rotation matrix, the above mentioned rotation matrix in Equation 4-3 has to be transposed, since it is an orthogonal matrix.

Then, based on the pre-processed exterior orientation parameters, the geometric relationship between imagery and point cloud data can be recovered, and these two data sets can be co-registered together. Before applying the proposed method onto the testing data set, the quality of co-registration has been checked beforehand by back-projecting laser points onto the corresponding image.

Figure 4.3 The back-projection result of direct geo-referenced data (red points are the back-projected laser points)

In Figure 4.3, the discrepancies between back-projected laser points (the front facade of the building) and their corresponding features on the image are obvious. Therefore, the proposed procedure is applied to the experimental data sets to estimate the bias from inaccurate platform orientation and to improve the co-registration quality.

On the other hand, due to the weather and the time when the images were captured, all the images acquired by this MLS platform looks dark. As a result, it may influence the accuracy of selected point features from images. So the brightness of each image has been adjusted before applying the proposed procedure. Because this process doesn't change the geometry of image, it won't have any impact on the result of the proposed procedure.

4.3.   Workflow

In this experimental test, first, the radial distortion of images is modelled and corrected in camera calibration step. Then, the selected images in the same block are relatively oriented and adjusted in a photogrammetric network. In this stage, the orientations of images are reconstructed in a local coordinate system. Subsequently, a multi-feature based similarity transformation is applied to reconstruct the camera's orientations in the mapping coordinate system. In this step, all the corresponding features from both images and point cloud data are manually selected. Therefore, to apply the point-based similarity transformation, at least three points in each adjusted image network should be identifiable in the corresponding point cloud data sets. For the extended plane-based transformation which includes point features and plane features, points from at least four intersecting planes should be extracted from the adjusted image network. These four planes should be also identifiable in the point cloud data. Finally, the estimation of bias on boresight angles and lever-arm offsets is modelled and calculated based on a comparison between the estimated EOPs and the original EOPs.

4.4.   Result of camera calibration

The camera calibration has been carried out by using the above mentioned method in Section 3.2. The intrinsic parameters of Camera 1 are estimated in the software "Image Modeller". The original and calibrated intrinsic parameters are shown in Table 4-1.

Table 4-1 The intrinsic parameters of Camera 1

	Principal Point_X	Principal Point_Y	Focal Length (mm)	K1	K2
Original	810.251 pix	614.302 pix	3.8664	-0.0156	0.0003
Calibrated	770.075 pix	621.840 pix	3.7546	-0.2150	0.0603

After radial distortion correction, the curved vertical structures are corrected. Figure 4.4 illustrates an image before and after radial distortion correction. The red arrow is a vertical line in the image. In the original image, the pole of the street lamp is obviously curved, whereas in the corrected image, the pole becomes vertical.

(a) (b)

Figure 4.4 (a) original image; (b) corrected image (clipped)

4.5. Result of feature-based co-registration method

After the correction of radial distortion, the relative orientation was carried out in each image block respectively. In each block, a free network adjustment was performed using all 10 images. To identify the orientation of each image, a local coordinate system was set up in the photogrammetric network, and then, the orientations of all the images in the same block were reconstructed in the same reference system. The relative orientation procedure was completed in the software of "Image Modeller". The conjugated target points were manually selected in the software, and these points were well-distributed in each image. In the meantime, additional points, especially point features like the corners of the man-made structure, which were also identifiable in the point cloud data, were selected in the image network. These points enable the 3D similarity transformation from image space to the object space. The network adjustment with an average of 30 to 40 points per image yielded an RMS value less than 0.5 pixels for each block.

4.5.1. Result of point-based transformation

In order to recover the exterior orientation parameters of each image, a feature-based 3D similarity transformation was applied in each image block based on the results obtained in the relative orientation stage. Just as it has been introduced in Chapter 3, first, a point-based similarity transformation was carried out to get an approximate estimation of the transformation from the orientated image space to the geo-referenced point cloud data. Table 4-2 illustrates the accuracy of the point-based similarity transformation from the image space to the object space.

Table 4-2 The result of the point-based 3D similarity transformation

Block	Number of Corresponding points	RMS_X (m)	RMS_Y (m)	RMS_Z (m)	RMS_XYZ (m)
1	7	0.0319	0.0325	0.0202	0.0498
2	7	0.0325	0.0300	0.0281	0.0524
3	9	0.0368	0.0266	0.0551	0.0714
4	7	0.0371	0.0333	0.0192	0.0534

In this table, RMS_XYZ means the rms distance between corresponding point features after applying the point-based 3D similarity transformation. RMS_X, RMS_Y and RMS_Z represent the rms discrepancy along each axis. These values are given in the mapping coordinate system.

There are two main error sources for the point-based similarity transformation. One is from the 3D points derived from the free network adjustment. Different points extracted from the adjusted photogrammetric network may have different accuracy. So, if some points with very low accuracy are involved in the point-based similarity transformation, the accuracy of transformation may be affected. The other error source is from the corresponding points extracted in the point cloud data. In this test, due to the property of point cloud data, it's very hard to find accurate point-to-point matches. Instead, the point closest to the estimated corresponding location was picked out in the point cloud data. This error depends on the resolution of the scanner.

Based on the error propagation law, the accuracy of 7 estimated transformation parameters derived from the point-based transformation can be calculated.

Table 4-3 The accuracy of 7 estimated transformation parameters in the point-based similarity transformation (3 rotation angles ω, φ, κ; 3 translation parameters x, y, z and 1 scale factor s)

Block	σ_ω ($\degree$)	σ_φ ($\degree$)	σ_κ ($\degree$)	σ_x (m)	σ_y (m)	σ_z (m)	σ_s/s (%)
1	0.6532	0.4813	0.6188	0.0536	0.0552	0.0566	0.7505
2	1.2056	0.5787	0.6303	0.0580	0.0550	0.0598	0.5875
3	1.0542	0.5271	0.5730	0.0836	0.0785	0.0799	0.8506
4	0.6875	0.6474	0.6532	0.0754	0.0695	0.0766	1.2395

4.5.2. The result of the extended plane-based transformation

Then, the extended plane-based method was performed to refine the approximate estimation. The transformation parameters derived from the point-based transformation were used as the initial values in this step. At least four intersecting planes are needed to reconstruct the 3D similarity transformation from the oriented image space to the object space. In these four intersecting planes, at most 2 planes may be parallel. Therefore, planes with different orientations are needed in this research. In this test, vertical planes on the facades of the building and horizontal planes on the ground are selected from point cloud data. Table 4-4 illustrates the accuracy of the extended plane-based method. The distance from points to the corresponding planes in each image block has an rms value less than 4 cm.

Table 4-4 The result of the extended plane-based transformation

Block	Number of points	Number of planes	rms distance from points to corresponding plane (m)
1	70	7	0.0213
2	83	11	0.0274
3	58	13	0.0342
4	38	6	0.0234

Comparing Table 4-4 with Table 4-2, it can be conclude that the extended plane-based transformation has a much better accuracy with a smaller rms value in each image block. Based on the error propagation law, the accuracy of 7 estimated transformation parameters derived from the extended plane-based transformation can be calculated.

Table 4-5 The accuracy of 7 estimated transformation parameters in the extended plane-based method

Block	σ_ω (°)	σ_φ (°)	σ_κ (°)	σ_x (m)	σ_y (m)	σ_z (m)	σ_s/s (%)
1	0.2104	0.1264	0.0790	0.0040	0.0036	0.0104	0.0670
2	0.3647	0.1062	0.0743	0.0013	0.0069	0.0209	0.0921
3	0.2053	0.1779	0.1092	0.0257	0.0164	0.0997	0.6675
4	0.3296	0.0980	0.0516	0.0164	0.0114	0.0112	0.3380

With a comparison between Table 4-3 and Table 4-5, it is easy to conclude that the extended plane-based method has much higher precision on all the 7 estimated transformation parameters in each image block. This result also proves that the proposed multi-feature based similarity transformation (first estimated by the point-based method, then refined by extended-plane based method) can achieve better estimation on the transformation parameters from the image space to the object space.

From Table 4-5, it's easy to observe that in each image block, the estimated rotation angle γ has the smallest standard deviation compared with another two rotation angles (ω, φ). This can be explained by analyzing the selection of plane features in the point cloud data. Because the experimental data sets were acquired in the urban area, the facades of the building are the most common plane features in the point cloud data. These plane features on man-made structures are usually vertical to the ground or the x-y plane in the mapping coordinate system. Considering the mathematical model of the plane-based transformation (see Equation 3-10), it can be found that these vertical planes with a normal vector in the form of $(a, b, 0)$ are directly associated with the coordinates in x-y plane. On the other hand, the rotation angle γ just represents the rotation in x-y plane (along Z axis). Therefore, with sufficient vertical planes extracted in the point cloud data, the rotation angle γ can be accurately estimated in each image block. To have an accurate estimation on another two rotation angles, planes with different orientations are needed (not vertical to the ground). However, in this test, except these vertical planes, only several horizontal planes on the ground are able to be extracted from the point cloud data (see Figure 4.5). As a result, another two rotation angles are with lower precision compared with the rotation angle γ in each image block. In the further research, besides common vertical and horizontal planes, additional inclined plane features are needed to guarantee the accuracy of the extended plane-based transformation.
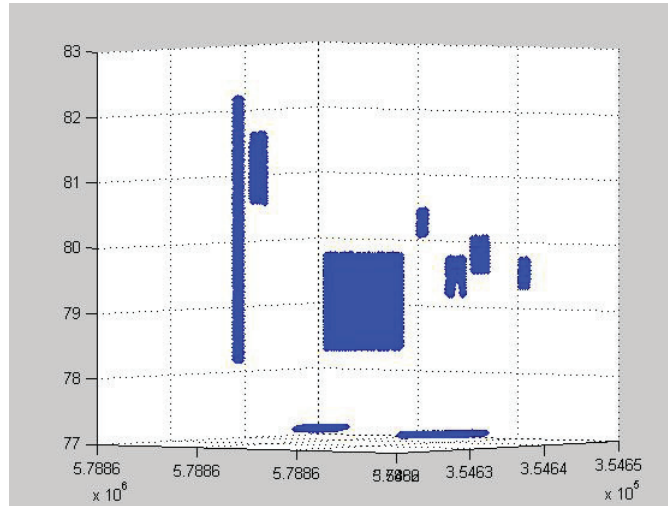
Figure 4.5 Selected plane features for block 2

Moreover, the same as the point-based similarity transformation, the accuracy of the estimated transformation parameters is also affected by the accuracy of 3D points which are derived from the adjusted photogrammetric network.

4.6. Result of bias estimation

Based on the recovered transformation from the image space to the object space, the exterior orientation parameters of each image can be reconstructed. Then, the estimation of the bias on boresight angles and lever-arm offsets can be solved with the mathematical model which utilizes both the estimated EOPs and the original EOPs together. In the previous stage, we have got two sets of estimated transformation parameters from the oriented image space to the object space: one is estimated from the point-based similarity transformation, and the other one is the refined transformation parameters derived from the extended plane-based method. To demonstrate the different performances of these two sets of transformation parameters, the bias estimation was carried out on both of them. The mathematical model used for the bias estimation in this test is introduced in Section 3.4.

4.6.1. Bias estimation based on the extended plane-based similarity transformation

First, the bias estimation is carried out based on the estimated EOPs derived from the extended plane-based method. To investigate the performance of estimated EOPs in different image blocks, the bias is first estimated in each image block separately. Then, a combined estimation which includes all the four image blocks is carried out to eliminate the correlations on different driving directions. Table 4-6 illustrates the results of estimated bias.

In Table 4-6, we could observe that there are obvious variations among the results of estimated bias in each image block. For example, the estimated bias on α varies from -0.8179 degree to -0.3492 degree. To explain this, we need look back to the accuracy of estimated transformation parameters in each image block, since the accuracy of estimated bias heavily relies on the accuracy of the reconstructed EOPs which are directly derived from the extended plane-based transformation. If the EOPs of each image are very badly estimated, the final estimation of bias cannot be accurate. In Table 4-5, we could notice that there is a low precision on the estimated rotation angles. This low precision is consistent with the variation of the estimated bias on boresight angles in different image blocks. Therefore, to reduce the variation between

different blocks and have a better estimation on the bias, the accuracy of the results of similarity transformation in previous stage has to be improved.

Meanwhile, it is also obvious that, compared with the estimated bias on boresight angles, the estimated bias on lever-arm offsets has a much larger variation among different image blocks. This is mainly because there are only three estimated rotation angles involved in the bias model on boresight angles, while all the 7 parameters estimated from similarity transformation are involved in the bias model on lever-arm offsets. Based on the error propagation law, all the errors from the 7 estimated parameters are directly propagated to final estimated bias on lever-arm offsets. Therefore, the estimated bias is more consistent on boresight angles than on lever-arm offsets.

Table 4-6 The result of bias estimation (based on the estimated EOPs derived from the extended plane-based method)

Block	α (°)	β(°)	γ(°)	Δx (m)	Δy (m)	Δz (m)
1	-0.8179	0.8138	-0.0685	0.0310	-0.0267	-0.0190
2	-0.9092	1.2565	0.1993	-0.0214	-0.0257	-0.0661
3	-0.6457	1.1196	0.2565	0.0976	0.0794	-0.0972
4	-0.3492	0.7924	0.1015	-0.0455	-0.0103	-0.0342
1-4	-0.6640	1.0567	0.1266	0.0144	0.0418	-0.0538

Moreover, we could find that in block 3, the estimated bias on lever-arm offsets is greatly different from the estimated result in other blocks. This result is also consistent with the accuracy analysis of the estimated transformation parameters in each block. In Table 4-5, it has been seen that in the extended plane-based transformation, block 3 has the lowest precision on 3 estimated translation parameters and the scale factor. For example, the estimated translation parameter Z in block 3 has a standard deviation around 10 cm which is ten times larger than the standard deviation in other 3 blocks. All these errors will directly propagate to the reconstructed EOPs of images and the estimated bias on lever-arm offsets in block 3. Therefore, an additional estimation is carried out only using block 1, block 2 and block 4.

Table 4-7 The result of bias estimation using image block 1, 2 and 4

Block	α (°)	β(°)	γ(°)	Δx (m)	Δy (m)	Δz (m)
1,2,4	-0.6701	0.9540	0.0833	-0.0120	-0.0209	-0.0398

Table 4-8 The accuracy of the estimated bias using image block 1, 2 and 4

Block	σ_α (°)	σ_β(°)	σ_γ(°)	$\sigma_{\Delta x}$ (m)	$\sigma_{\Delta y}$ (m)	$\sigma_{\Delta z}$(m)
1,2,4	**0.2865**	0.2620	0.1704	0.0637	0.0646	0.0663

Table 4-8 illustrates the accuracy of the estimated bias using block 1, 2 and 4. It has been seen that the standard deviation of the estimated lever-arm bias is around 6 cm. The maximum standard deviation of the estimated bias on boresight angles is 0.2865 degree. This will introduce an error around 5 cm in the object space for a distance of 10 m.

4.6.2. Bias estimation based on the point-based similarity transformation

To make a further assessment of the estimated bias based on the extended plane-based transformation, the bias estimation is also carried out on the EOPs derived from point-based similarity transformation. The set up of bias estimation is the same as above test.

Table 4-9 The result of bias estimation (based on the EOPs derived from point-based similarity transformation)

Block	α (°)	β(°)	γ(°)	Δx (m)	Δy (m)	Δz (m)
1	0.0346	0.3122	0.3784	-0.0142	0.0305	0.0231
2	-0.2744	1.0640	0.3630	-0.0126	0.0544	-0.0389
3	-0.0773	0.6532	0.2347	0.0630	0.0515	-0.0613
4	0.0462	0.7924	0.0996	0.0517	0.0116	0.0378
1-4	-0.0677	0.7053	0.2689	0.0220	0.0370	-0.0098

Comparing Table 4-9 with Table 4-6, it can be concluded that the plane-based method has more consistent estimated bias in each image block. This result is consistent with the accuracy analysis of point-based transformation and the extended plane-based transformation. It also proves that estimated bias can be more reliable based on the EOPs reconstructed in the extended plane-based method.

Table 4-10 The accuracy of the estimated bias using image block 1 to 4

Block	σ_α (°)	σ_β(°)	σ_γ(°)	$\sigma_{\Delta x}$ (m)	$\sigma_{\Delta y}$ (m)	$\sigma_{\Delta z}$(m)
1,2,4	0.3552	**0.3564**	0.2117	0.0875	0.0868	0.0835

Table 4-10 gives the accuracy of the estimated bias using all the 4 image blocks based on the result of point-based transformation. With a comparison between Table 4-8 and Table 4-10, it is easy to conclude the estimated bias based on the plane-based transformation is more accurate.

Based on above analysis, it can be concluded that, in this proposed two-step procedure, the accuracy of the estimated bias on boresight angles and lever-arm offsets heavily depends on the quality of EOPs reconstructed in the co-registration stage. Therefore, to improve the final result of the estimated bias, more accurate transformation parameters for reconstructing the EOPs of the camera have to be determined.

4.7. Examination of the estimated bias

In this section, the performance of the estimated bias will be evaluated. The estimated bias shown in Table 4-7 (derived from the extended-plane based method and only using block 1, block 2 and block 4) will be used to correct the original EOPs provided by the MLS platform. Then, the co-registration quality between the image and the point cloud data will be evaluated based on the corrected EOPs.

4.7.1. Visual Examination

Equation 3-27 has given the mathematical model for the co-registration between imagery and geo-referenced point cloud data. Therefore, by using the corrected EOPs, the geo-referenced point cloud data can be directly transformed from the mapping coordinate system to the image coordinate system. Then

the co-registration quality between imagery and point cloud data can be evaluated in the image space based on the comparison between back-projected laser points and the corresponding images.

As expected, if the relative geometric relationship between the image and the geo-referenced point cloud data has been very accurately determined, the back-projected laser points should match the corresponding features on the image perfectly. Therefore, the visual examination method is an efficient way to check the co-registration quality between the back-projected laser points and the images.

In this research, the test data is taken at the urban area, so, the man-made structures which usually have regular shapes are the most common features in the point cloud data. Compared with vegetations and other irregular-shaped features, these man-made structures have several advantages. The first is these features can be easily detected and extracted from point cloud data based on the segmentation algorithms. The second is the discrepancies between regular-shaped features can be easily observed in the visual examination. Therefore, the man-made structures, like the facade of a building and a wall, can be mainly used for the evaluation of co-registration qualities in the visual examination. In the meantime, considering the back-projection procedure is from the 3D object space to the 2D image space, to have a better evaluation on the co-registration quality, plane features with different orientations and positions in the 3D object space are needed. In this research, there are three main types of plane features selected in the point cloud data for the visual examination. The first type is the plane features parallel to the driving direction of the MLS platform, and in the test data sets, most of the front facades of the buildings are this type of plane features. The second type is the plane features perpendicular to the driving direction. The third type is the plane features on the ground or parallel to the ground plane. The three types of plane features are illustrated in Figure 4.6.
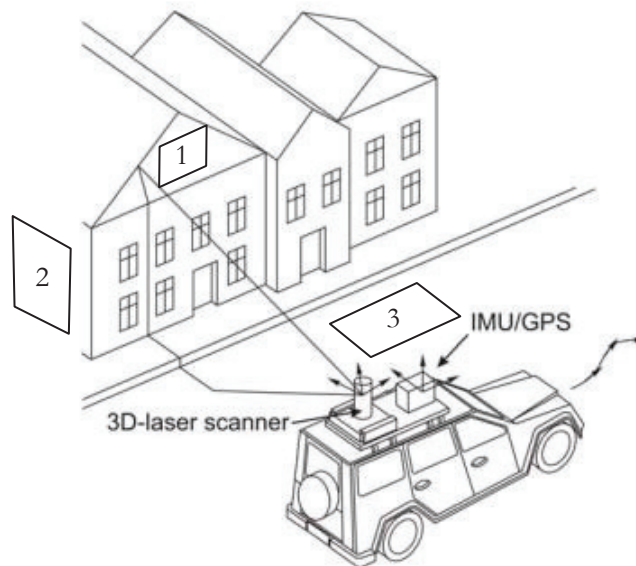
Figure 4.6 Three different types of plane features used for co-registration quality evaluation (Rieger et al., 2008)

4.7.2. Error analysis of the back-projected laser points

Based on the error propagation law, the error of the estimated bias will directly propagate to the back-projected laser point. To compute the error budget of the back-projected laser points in the image coordinate system, the collinearity equations for co-registration between the image and the point cloud data (given as Equation 3-27) have to be linearized by a first-order Taylor series expansion. After applying

the error propagation law onto the covariance matrix of the error sources (the estimated bias on both boresight angles and lever-arm offsets), the covariance matrix of the back-projected laser point can be described as:

$$C_i = J \cdot C \cdot J^T$$

<div align="right">Equation 4-4</div>

Where C_i is the covariance matrix of the coordinates of back-projected laser point (a 2 x 2 matrix), C is the covariance matrix of the estimated bias (a 6 x 6 matrix), and J is the Jacobian matrix which consists of the partial derivatives with respect to the different variables (estimated bias) in the collinearity equations.

4.7.3.   Result of the co-registration between selected features and the image

To examine performance of the estimated bias, one image is randomly selected to analyze. Three different plane features, which just correspond to the three different types of plane features introduced in the previous section, are also selected from the point cloud data. For each selected plane feature, the laser points will be back-projected and superimposed with the image, and then the co-registration quality between the image and different plane features will be evaluated via visual examination. In the following paragraph, the result of co-registration will be illustrated.

<div align="center">(a)   (b)</div>

Figure 4.7 The co-registration between image and the first-type plane feature (a) is the back-projection result using the original EOPs; (b) is the result using corrected EOPs

First, a plane feature which is parallel to the driving direction of the platform is selected for the visual examination. Figure 4.7 illustrates the co-registration results before and after correcting the original EOPs. In Figure 4.7 (a), the yellow lines represent the line features in the image, and the blue lines represent the corresponding lines in the back-projected laser points. It is easy to observe that before correcting the estimated bias on boresight angles and lever-arm offsets, there are obvious discrepancies between images and the point cloud data along the driving direction. In the meantime, we could also find that after correction on the original EOPs, the selected plane feature matches the corresponding facade of the building on the image well.
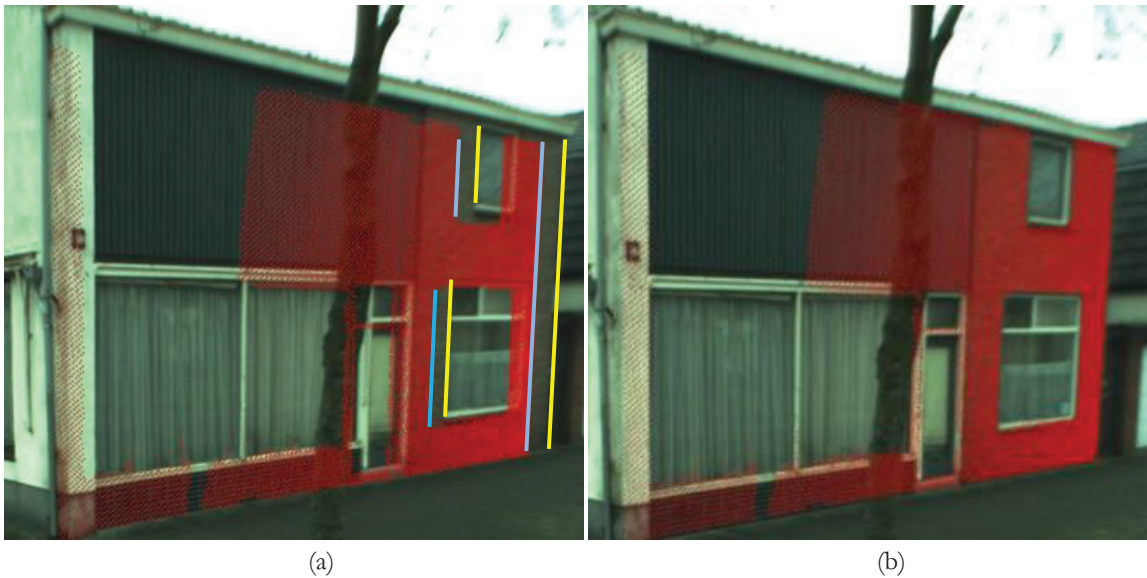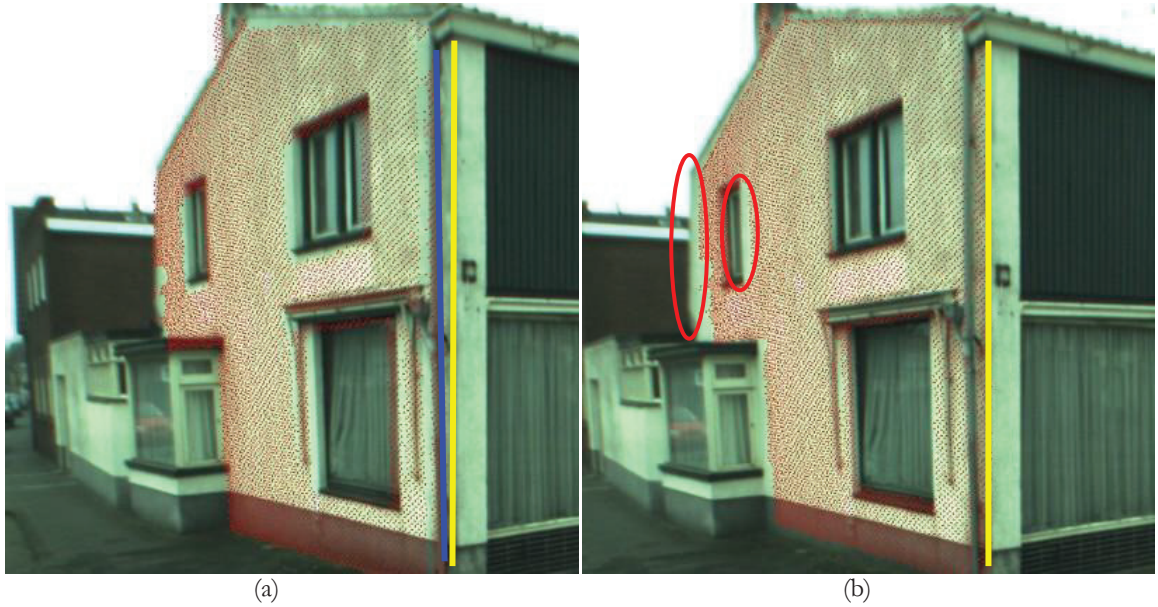
<div align="center">(a)   (b)</div>

Figure 4.8 The co-registration between image and the second-type plane feature (a) is the back-projection result using the original EOPs; (b) is the result using corrected EOPs

Figure 4.8 illustrates the co-registration result of the selected plane feature which is perpendicular to the driving direction. We could observe that after the correction, some parts of back-projected laser points match the image well, especially those points close to the platform. Figure 4.8(a) is the back projection result before correction, an obvious discrepancy between the back-projected laser point and the image has been specified by the blue and yellow lines. In Figure 4.8 (b), we can observe that on the same line, there is a good co-registration quality after the correction. However, for those points farther away from the platform, there are still obvious discrepancies between the back-projected laser points and the image (specified by the red circles in Figure 4.8(b)).

To make a further assessment of the co-registration quality between the selected plane feature and the image, several laser points on the plane feature are selected and the distances from the back-projected laser points to the corresponding line features are calculated on the image. In the meantime, the error budgets of these back-projected points are also calculated via Equation 4-4.

<div align="center">Table 4-11 Accuracy assessment of co-registration</div>

Line feature on the image	Number of back-projected points in	Average distance from point to line	Average error budget on X axis	Average error budget on Y axis
1	7	8.90 pixels	8.51 pixel	6.13 pixels
2	12	4.17 pixels	4.97 pixels	5.42 pixels

In Table 4-11, the selected feature 1 is away from the platform and the feature 2 is close to the platform. We could find that feature 1 has a larger average distance as well as large error budgets on each back-projected laser points. As for feature 2, the average distance from back-projected points to the line is smaller, and the error budgets on each point are also smaller. This result indicates that, on this selected plane feature, laser points closer to the platform may have a better co-registration quality as well as smaller error budgets. This result is consistent with the observation of co-registration in Figure 4.8(b).

<div align="center">(a)   (b)</div>

Figure 4.9 The co-registration between image and the selected plane feature on the ground (a) is the back-projection result using the original EOPs; (b) is the result using corrected EOPs

Figure 4.9 illustrates the co-registration result between the image and the selected plane feature on the ground. The discrepancy between back-projected laser points and the image has been specified in Figure 4.9(b). The back-projected laser points along the edge of the road (specified by the blue line in Figure 4.9(b)) have a large error budget around 8 pixels on each axis. This is also consistent with the observation by visual examination.

In this section, the performance of the estimated bias has been evaluated. Based on the co-registration result between the image and the point cloud data, we can find that due to the accuracy of the estimated bias, the final co-registration quality is not as good as expected. Even after the correction, there are still obvious discrepancies between the back-projected laser points and the image. By considering the error propagation law, the error budget of the back-projected laser points can be calculated. The result of error budget is consistent with the observation in the visual examination. Therefore, to have a better co-registration quality between the image and the point cloud data, more accurate estimated bias on boresight angles and lever-arm offsets are needed.

4.8. Summary

In this chapter, the proposed two-step procedure has been tested on the selected experimental data sets. In the first step of the proposed procedure, the EOPs of the camera at each exposure moment are reconstructed through two different methods (point-based method and the extended plane-based method). The accuracy of the estimated transformation parameters derived from each method has been analyzed in this step. The final result demonstrates that compared with the traditional point-based method, the extended plan-based method proposed in this research has a better performance for the estimation of transformation parameters on the actual applications. Then, in the second step, the bias of boresight angles and lever-arm offsets is estimated based on the reconstructed EOPs in the previous stage. Although the final result of the estimated bias is affected by the accuracy of the reconstructed EOPs and may not be very accurate in this research, the potential of this proposed procedure on actual applications has been demonstrated in this experimental test. In the meantime, the accuracy analysis on estimated bias is also carried out based on the error propagation law. From this analysis, we can find that both the errors from the selected tie points which are derived from the adjusted photogrammetric network for the

similarity transformation and the selection of plane features in the point cloud data will directly affect the final accuracy of the estimated bias. As a result, we are able to get more ideas on how to improve the accuracy of the final result in the further research.

The performance of the estimated bias is also evaluated in this research. By using the corrected EOPs of the image, the laser points are able to be back-projected onto the corresponding image, and the co-registration quality between the back-projected laser points and the image can be assessed in the image space. As expected, if the estimated bias is accurate enough, there will be a good co-registration quality between the back-projected laser points and the image. In this research, visual examination and error analysis are carried out to evaluate the co-registration quality using the EOPs which are corrected by the estimated bias. In the visual examination method, three different types of plane features are selected in the point cloud data and back-projected to the image, and then the co-registration quality on each selected plane feature will be evaluated. In the error analysis, based on the error propagation law, the error budgets on the back-projected laser points can be calculated. In this experimental test, the estimated errors on boresight angles have a standard deviation around 0.2 degrees, and the estimated errors on the lever-arm offsets have a standard deviation around 6 cm. This result is not accurate enough. In the result of visual examination, obvious discrepancies between the back-projected laser points and the image can be still observed. In the meantime, the error budgets of those back-projected laser points with large discrepancies are also calculated. The result of the error budgets is consistent with the observations in the visual examination. Therefore, based on this analysis, it can be concluded that, to have a better co-registration quality between the image and the point cloud data, the accuracy of the estimated bias on boresight angles and lever-arm offsets has to be improved in further research.

5.   CONCLUSION AND RECOMMENDATIONS

5.1.   Conclusion

The main objective of this research is to develop a procedure to model and correct the potential error sources which may influence the co-registration quality in an inaccurately calibrated MLS platform. This procedure is fulfilled in a two-step solution. In the first step, a multi-feature based co-registration method is developed. By using this method, the orientations of the camera can be reconstructed with respect to the geo-referenced point cloud data. In the second step, with utilizing both the reconstructed EOPs of the camera obtained in the first step and the original EOPs provided by the platform together, the bias on the boresight angles and the lever-arm offsets of the camera can be estimated respectively. By using the estimated bias, the original EOPs of the camera can be corrected, and the point cloud data and imagery can be registered into the same coordinate system.

The performance of the proposed procedure is then tested. The experimental data set for this test includes 4 small image blocks acquired on different driving directions and the corresponding point cloud data covered the same area. Both the imagery and point cloud data were acquired by the same MLS platform in the same survey project. In this research, the accuracy analysis is carried out on each step. The co-registration quality between imagery and point cloud data is also examined with the corrected EOPs of the camera. Although in this research, the accuracy of the final estimated bias is not very high, and the co-registration quality between the image and the point cloud data is not as good as expected. The whole work in this research still demonstrates the possibility of applying the proposed procedure to actual applications. Several conclusions can be drawn based on the analysis of the result.

- Based on the proposed co-registration method, the orientations of the camera can be reconstructed in the mapping coordinate system by a relative-absolute orientation. The test on the experimental data has demonstrated the feasibility of this proposed co-registration method.
- Since the orientations of the camera are reconstructed by a relative-absolute orientation, the accuracy of the relatively oriented images in the photogrammetric network needs to be evaluated. Based on the error propagation law, all the errors from this stage will affect the accuracy of the reconstructed EOPs of the camera, and directly propagate to the final result of the estimated bias.
- In the absolute orientation stage, the accuracy of the point-based similarity transformation and the extended plane-based transformation has been analyzed. The accuracy analysis demonstrates that the extended plane-based transformation has a much better performance on actual applications.
- Based on the accuracy analysis of the extended plane-based transformation, it can be also concluded that the selection of the plane features in the point cloud data may influence the accuracy of estimated 3D transformation parameters. In this research, because most of the selected plane features are vertical to the ground, the two estimated rotation angles along x-axis and y axis have a lower precision. To have a better estimation on the transformation parameters, plane features with different orientations are needed.
- Just like other 2-step calibration methods, in this proposed two-step procedure, the quality of the estimated bias is heavily dependent on the quality of reconstructed EOPs. To improve the accuracy of the estimated bias, the accuracy of transformation parameters in the previous co-registration step has to be improved.

5.2.   Answers to the research questions

1.   How to check the error from image distortion?

To eliminate the effect of image distortion, the camera intrinsic parameters are corrected in a camera self-calibration procedure. In this procedure, the radial distortion of the camera lens is modeled and corrected.

2.   How to recover the exterior orientation parameters of imageries based on point features?

In this research, the exterior orientation parameters of the image are determined with a relative-absolute orientation. First, the image will be oriented and adjusted in a photogrammetric network. The coordinates of tie points and the orientations of the camera are reconstructed in a local coordinate system. Then at least 3 pairs of corresponding points from both the image and the point cloud data are needed to complete the absolute orientation from the local coordinate system to the mapping coordinate system. Based on the same transformation, the orientations of the image given in the local coordinate system can be transformed into the mapping coordinate system. Then the exterior orientation parameters of the image can be reconstructed.

3.   How to recover the exterior orientation parameters of imageries based on line features?

The same as the point-based method, first the images are adjusted and oriented in a photogrammetric network. Then at least 2 non-intersecting line features are needed to complete the 3D similarity orientation from the local coordinate system to the mapping coordinate system. In the meantime, because a 3D line in the point cloud data can be represented by the intersection of two adjacent planes, in this research, the line-based transformation can be also solved by using an extended plane-based method.

4.   How to recover the exterior orientation parameters of imageries based on plane features

Similarly, first the images are adjusted and relatively oriented in a local coordinate system. Then, points from the adjusted image network and the corresponding planes from the point cloud are needed to solve the transformation from the local coordinate system to the mapping coordinate system. In the proposed plane-based transformation method, at least three points for each plane and at least four intersecting planes are needed. Among these four intersecting planes, at most two planes can be parallel. Meanwhile, because one 3D line or one 3D point could be represented by the intersection of two planes or three planes respectively, the point-based and line-based methods could be extended to the plane-based method as well. One 3D point can establish 3 equations, and one 3D line can establish 2 equations for the plane-based transformation.

5.   What is the result of applying plane features in this proposed procedure?

In the test, the transformation parameters from the oriented image space to the object space are first estimated with a point-based transformation. Then, the plane-based transformation is used to refine the approximately estimated transformation parameters derived in previous stage. The result of the transformation illustrates that, after introducing the plane features, the accuracy of the estimated transformation parameters has been improved. This result also demonstrates the possibility of using plane features in actual application.

6.   How to model the systematic errors caused by inaccurate platform orientation?

In this research, the bias on the boresight angles and the lever-arm offsets are modeled separately. Both the reconstructed EOPs derived from the proposed co-registration method and the original EOPs provided by the MLS platform are utilized together to solve the estimated bias.

7. How to evaluate the estimated bias derived in the proposed procedure?

The accuracy analysis is carried out on every stage in this research. Based on the error analysis, it can be concluded that all the errors from camera calibration to the proposed co-registration method will directly prorogate to the final result of the estimated bias. In this research, the estimated bias on boresight angles has a standard deviation around 0.2 degrees, and the estimated bias on the lever-arm offsets has a standard deviation around 6 cm. To verify the performance of the estimated bias, first the original EOPs of the image have to be corrected with the estimated bias. Then, the point cloud data needs to be back-projected into the image space based on the corrected EOPs. The back-projection result is evaluated by visual examination and error analysis. The observations in the visual examination are consistent with the results of error analysis.

5.3.   Recommendations

The following are some recommendations of this research:

- In this research, the radial distortion of the image is modelled and corrected in a self-calibration procedure. However, the accuracy of this calibration procedure is not very well evaluated. Considering the error from camera calibration will directly influence the accuracy of the proposed co-registration method and the final estimated bias, a more accurate camera calibration step may be carried out for further research.

- In this research, to complete the 3D similarity transformation from the oriented image space to the object space, some tie points which can be also identifiable in the point cloud data are needed. However, the accuracy of these selected tie points is not very well evaluated in the local coordinate system. The accuracy of these selected tie points for the similarity transformation needs to be controlled for further research.

- When applying the plane-based transformation method to refine the estimated transformation parameters, the final accuracy is limited by the selection of plane features in the point cloud data. In this research, because most of the selected plane features are vertical to the ground plane, the precision of two estimated rotation angles along X-axis and Y-axis is low. In the further research, besides common vertical and horizontal planes, additional inclined plane features are recommended to improve the accuracy of the extended plane-based transformation.

- For further research, automatic co-registration method between imagery and point cloud data can be investigated.

LIST OF REFERENCES

Al-Manasir, K., & Fraser, C. S. (2006). Registration of terrestrial laser scanner data using imagery. *The Photogrammetric Record, 21*(115), 255-268.

Ayache, N., & Faugeras, O. D. (1989). Maintaining representations of the environment of a mobile robot. *Robotics and Automation, IEEE Transactions on, 5*(6), 804-819.

Bäumker, M., & Heimes, F. (2001). *New calibration and computing method for direct georeferencing of image and scanner data using the position and angular data of an hybrid inertial navigation system.* Paper presented at the Proc. of the OEEPE Workshop 2011, Hanover.

Casella, V., Galetto, R., & Franzini, M. (2006). An Italian Project on the Evaluation of Direct Georeferencing in Photogrammetry. *Proceedings Eurocow.*

Cologne, U. o. (2012). Radial Distortion Correction Retrieved 1/25/2012, 2012, from http://www.uni-koeln.de/~al001/radcor_files/hs100.htm

Cramer, M., & Stallmann, D. (2002). System calibration for direct georeferencing. *International Archives of Photogrammetry Remote Sensing and Spatial Information Sciences, 34*(3/A), 79-84.

Cramer, M., Stallmann, D., & Haala, N. (1998, April 21-23). *Sensor integration and calibration of digital airborne three-line camera systems.* Paper presented at the International Workshop on Mobile Mapping Technology, Bangkok, Thailand.

Cramer, M., & Tuttgart, S. (1999). *Direct Geocoding-is Aerial Triangulation Obsolete?* Paper presented at the 47th Photogrammetric Week (Eds. Fritsch/Spiller), Wichmann Verlag.

El-Sheimy, N. (1992). A mobile multi-sensor system for gis application in urban centers. *Int. Arch. Photogramm. Remote Sens, 31*, 95-100.

Fraser, C. S. (1997). Digital camera self-calibration. *ISPRS Journal of Photogrammetry and Remote Sensing, 52*(4), 149-159.

González-Aguilera, D., Rodríguez-Gonzálvez, P., & Gómez-Lahoz, J. (2009). An automatic procedure for co-registration of terrestrial laser scanners and digital cameras. *ISPRS Journal of Photogrammetry and Remote Sensing, 64*(3), 308-316. doi: 10.1016/j.isprsjprs.2008.10.002

Grejner-Brzezinska, A. (2001). Direct Sensor Orientation in Airborne and Land-based Mapping Applications (T. O. S. U. Department of Civil and Environmental Engineering and Geodetic Science, Trans.) (pp. 46-47). Columbus, Ohio: Report.

Haala, N., Peter, M., Cefalu, A., & Kremer, J. (2008, 20 - 25 October). *Mobile lidar mapping for urban data capture.* Paper presented at the VSMM 2008 - Conference on Virtual Systems and MultiMedia Dedicated to Digital Heritage, Limassol, Cyprus.

Habib, A. F., Kersting, A. P., & Bang, K. I. (2010, 15-18 June). *Comparative Analysis of Different Approaches for the Incorporation of Position and Orientation Information in Integrated Sensor Orientation Procedure.* Paper presented at the Proceedings of Canadian Geomatics Conference 2010 and ISPRS Commision I Symposium, Calgary, AB, Canada.

Habib, A. F., Kersting, A. P., Ruifang, Z., Al-Durgham, M., Kim, C., & Lee, D. (2008). LiDAR strip adjustment using conjugate linear features in overlapping strips. *International Archives of Photogrammetry, Remote Sensing and Spatial Information Sciences*, 3-11.

Honkavaara, E., Ilves, R., & Jaakkola, J. (2003, 22-23 September). *Practical results of GPS/IMU/camera system calibration.* Paper presented at the Proceddings of International Workshop: Theor, Technology and Realities of Inertial/GPS Sensor Orientation, Castelldefels, Spain.

Jacobsen, K. (1999). *Determination of Image Orientation Supported by IMU and GPS.* Paper presented at the Joint Workshop of ISPRS Working Groups Hannover.

Jaw, J., & Chuang, T. (2008). Feature-based registration of terrestrial lidar point clouds. *The International Archives of the Photogrammetry, Remote Sensing and Spatial Information Sciences, 37*, 303-308.

Jaw, J., & Chuanga, T. (2010). *On the Effectiveness of Feature-based LIDAR Point Cloud Registration*. Saint-Mandé, France.

Kaasalainen, S., Kaartinen, H., Kukko, A., Anttila, K., & Krooks, A. (2011). Brief communication "Application of mobile laser scanning in snow cover profiling". *The Cryosphere, 5*(1), 135-138. doi: 10.5194/tc-5-135-2011

King, B. (1993). Optimisation of Bundle Adjustments for Stereo Photography. *International Archives of Photogrammetry and Remote Sensing, 29*, 168-168.

Lerma, J. L., Navarro, S., Cabrelles, M., & Seguí, A. E. (2010). Camera calibration with baseline distance constraints. *The Photogrammetric Record, 25*(130), 140-158.

Liu, J., Wang, D., Wang, H., & Fan, Y. (2011). *A Rigorous Approach for IMU Boresight Misalignment Calibration*.

Manandhar, D., & Shibasaki, R. (2000, 4-8 December). *Georeferencing of multi-sensor range data for vehicleborne laser mapping system (VLMS)*. Paper presented at the 21st Asian Conference on Remote Sensing (ACRS), Taipei.

Mostafa, M. M. R., & Schwarz, K.-P. (2001). Digital image georeferencing from a multiple camera system by GPS/INS. *ISPRS Journal of Photogrammetry and Remote Sensing, 56*(1), 1-12. doi: 10.1016/s0924-2716(01)00030-2

Optech. (2012). Optech Official Website Retrieved 31 January, 2012, from www.optech.ca

Pinto, L., & Forlani, G. (2002). *A single step calibration procedure for IMU/GPS in aerial photogrammetry*. Paper presented at the International Archives of Photogrammetry and Remote Sensing.

Rönnholm, P., Hyyppä, H., Hyyppä, J., & Haggrén, H. (2009). Orientation of airborne laser scanning point clouds with multi-view, multi-scale image blocks. *Sensors, 9*(8), 6008-6027.

Rau, J. Y., Habib, A. F., Kersting, A. P., Chiang, K. W., Bang, K. I., Tseng, Y. H., & Li, Y. H. (2011). Direct Sensor Orientation of a Land-Based Mobile Mapping System. *Sensors, 11*(7), 7243-7261.

Rieger, P., Studnicka, N., Pfennigbauer, M., & Zach, G. (2008). Boresight alignment method for mobile laser scanning systems. *Proceedings RSPRS, Moskau*.

Skaloud, J. (1999). *Optimizing georeferencing of airborne survey systems by INS/DGPS*. Ph.D, The University of Calgary.   (UGGE Report No. 20126)

Smith, M. J., Qtaishat, K. S., Park, D. W. G., & Jamieson, A. (2006). *IMU and Digital Aerial Camera Misalignment Calibration*. Paper presented at the Proceedings EuroCow, Castelldefels, Spain.

Vosselman, G., & Maas, H. G. (2010). *Airborne and terrestrial laser scanning*. Boca Raton: CRC.

Yastikli, N., & Jacobsen, K. (2005). Direct Sensor Orientation for Large Scale Mapping—Potential, Problems, Solutions. *The Photogrammetric Record, 20*(111), 274-284.